



STScI | SPACE TELESCOPE
SCIENCE INSTITUTE

When there is a discrepancy between the information in this technical report and information in JDox, assume JDox is correct.

JWST TECHNICAL REPORT

Title: Verifying the NIRSpec Wavelength Calibration and Resolving Power for Multi-Object Spectroscopy	Doc #: JWST-STScI-009239, SM-12 Date: 17 November 2025 Rev: -
Authors: Kayli Glidic, Phone: 410-338-4852 Tony Keyes, Peter Zeidler, James Muzerolle Page, Patrick Ogle, and Dan Coe	Release Date: 22 December 2025

1 Abstract

NIRSpec's Multi-Object Spectroscopy (MOS) mode uses an instrument model that maps detector coordinates to sky position and wavelength. This model was calibrated during commissioning using lamps to obtain an internal wavelength accuracy of approximately $\sim 1/10$ of a resolution element for any slitlet in the Micro-Shutter Assembly (MSA). However, this accuracy has not yet been fully verified across the entire MSA field of view (FOV) using observations of an external calibrator. Using Cycle 3 observations of a spatially unresolved planetary nebula in M31 (Program ID 06442), we assess the wavelength calibration accuracy for the following filter-disperser combinations: F100LP/G140M, F100LP/G140H, F170LP/G235M, F170LP/G235H, F290LP/G395M, F290LP/G395H, and CLEAR/PRISM. We centered the target in six micro-shutters across the MSA to determine the field dependence on the wavelength solution. In total, we used three distinct points for each grating and six for the PRISM. We find that all but one configuration achieves wavelength calibration accuracy within $\sim 1/10$ of a resolution element, though there may be systematic trends or offsets at lower levels. One PRISM observation shows larger offsets and will require follow-up observations to confirm whether that reflects a position dependence. All measurements indicate resolving powers that exceed pre-launch expectations, primarily due to the observatory's superb optical performance.

2 Introduction

The *Near Infrared Spectrograph* (NIRSpec) aboard the *James Webb Space Telescope* (JWST) supports four observing modes that cover a spectral range of 0.6–5.3 μm using seven dispersive elements: three high-resolution gratings, three medium-resolution gratings, and one PRISM. Table 2.1 lists all NIRSpec-supported filter–grating configurations, along with their nominal resolving powers and approximate wavelength ranges (JWST User Documentation, 2016–). The resolving power (R) is defined as

$$R = \frac{\lambda}{\Delta\lambda} \quad (1)$$

where λ is the wavelength, and $\Delta\lambda$ is the smallest resolvable difference in wavelength.

Operated by the Association of Universities for Research in Astronomy, Inc., for the National Aeronautics and Space Administration under Contract NAS5-03127

Check with the JWST SOCCER Database at: <https://soccer.stsci.edu>

To verify that this is the current version.

Table 2.1: Available disperser-filter combinations

Disperser-Filter Combination	Nominal Resolving Power	Wavelength Range † (μm)
G140M/F070LP	~1,000	0.70–1.27
G140M/F100LP		0.97–1.84
G235M/F170LP		1.66–3.07
G395M/F290LP		2.87–5.10
G140H/F070LP	~2,700	0.81–1.27
G140H/F100LP		0.97–1.82
G235H/F170LP		1.66–3.05
G395H/F290LP		2.87–5.14
PRISM/CLEAR	~100	0.60–5.30

† This table is from the JWST User Documentation. Resolving powers are calculated assuming a fully illuminated aperture and a resolution element size, $\Delta\lambda$, of 2.2 pixels (JWST User Documentation, 2016–).

Multi-Object Spectroscopy (MOS) with the *Micro-Shutter Assembly* (MSA) is one of the more complex observing modes for NIRSpec, featuring ~250,000 individually operable shutters that enable simultaneous spectral observations of multiple targets within a $3.6' \times 3.4'$ field of view (FOV). This mode, while it provides multiplexing spectroscopic capabilities, also introduces unique challenges, specifically for wavelength calibration, the accuracy of which is crucial for a broad range of measurements, including line identification, redshifts, and radial velocities. However, the vast number of possible shutter-disperser configurations combined with the additional complication of the grating wheel assembly (GWA) tilt makes a direct wavelength calibration approach impractical for MOS. The GWA has limited angular positioning repeatability, so each time the wheel moves, the optical element sits at a slightly different position, causing spectra on the detector to shift by small amounts in both the dispersion and cross-dispersion directions (JWST User Documentation, 2016–).

To address these challenges, NIRSpec uses a parametric instrument model (consisting of three parts: the FORE optics, the spectrograph, and the GWA), calibrated during commissioning with an internal accuracy of approximately 1/10 of a resolution element (0.2 pixels), to generate wavelength solutions for all configurations (Birkmann et al., 2011; Lützgendorf et al., 2022). To mitigate the GWA's non-repeatability, the model incorporates a correction from two tip/tilt sensors that monitor the angular displacement of the selected optical element whenever the wheel moves. The calibration of these sensors is also tracked monthly through a dedicated monitoring program, with preliminary results suggesting it is stable (JWST User Documentation, 2016–).

Nevertheless, the model's internal accuracy has not yet been fully verified across the entire MSA FOV using observations of an external calibrator. Therefore, this technical report aims to assess the wavelength calibration accuracy across the most used filter–grating combinations, as a function of wavelength and MSA field position, to better tie down the calibrations between the PRISM and the gratings and to identify any residual field dependence not captured by the instrument model. We exclude the filter F070LP configurations from this analysis for now because they are less often used and were a lower priority. Additionally, we also examine the resolving power for a point source as a function of wavelength and MSA field position.

The remaining structure of this report is as follows: Section 3 describes the observations used in this analysis. Section 4 outlines the line fitting analysis process. Section 5 presents the results. Finally, Section 6 summarizes our findings.

3 Observations

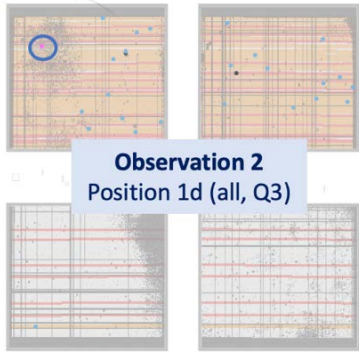
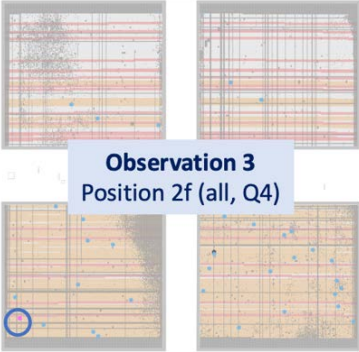
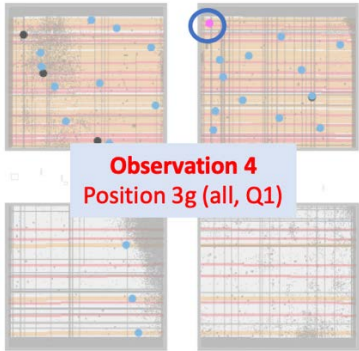
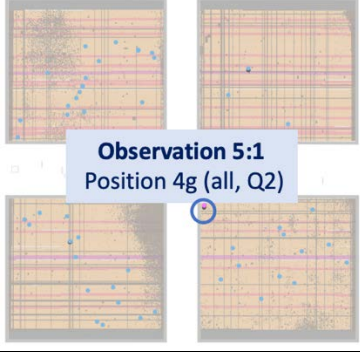
We utilize a series of MOS observations of a spatially unresolved planetary nebula in M31 (M31_PN2538; Simbad ID: [MMD2006] 2538), obtained as part of the Cycle 3 Calibration Program 06642 (PI: Muzerolle Page). The target (PN2538; Galera-Rosillo et al., 2022) was selected based on several criteria: its distance, which ensures no measurable spatial extension with JWST; its relative brightness compared to other M31 candidates, which minimizes exposure times; and its location in the outer region of M31, which minimizes source crowding critical for a successful target acquisition (TA/MSATA).

Due to a lack of precise astrometry and near-infrared photometry for the source, we first obtained *Near Infrared Camera* (NIRCam) pre-images, from which we could measure the target and reference star positions and brightness for MSATA. We also obtained an intermediate *fixed slit* (FS) observation using the S200A1 slit with the PRISM to confirm line fluxes before finalizing the MOS plans.

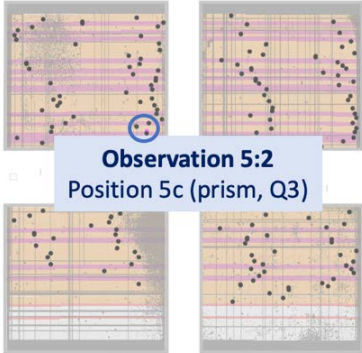
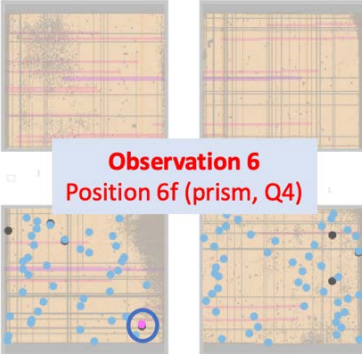
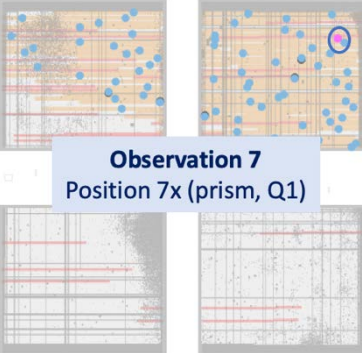
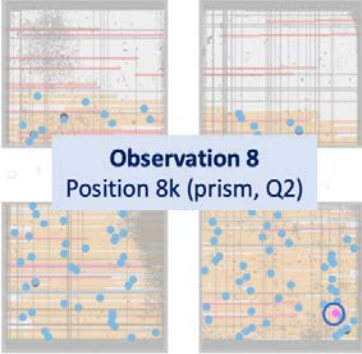
The MOS observations design aimed to observe the same object, centered in a 3-shutter slitlet, at multiple shutter locations for all dispersers. Initially, this program planned to observe the target at four MSA field positions (different MSA shutters) with all gratings and an additional four positions with the PRISM. However, Observation 4 failed due to an incorrect pointing caused by a ground system error. Additionally, in Observation 6, the source landed in a failed closed shutter. We also included several other filler targets in the field (between 26 and 151 targets for a given observation), selected by colors as possible giant stars. Those, however, are not considered in this analysis.

The MOS observations were taken between November 21, 2024, and January 20, 2025. Table 3.1 presents the details of each MOS observation.

Table 3.1: Program 06642 Observation Summary

Observation	Quadrant	Filter/Grating(s)	MSA Location
2	3	CLEAR/PRISM F100LP/G140M F100LP/G140H F170LP/G235M F170LP/G235H F290LP/G395M F290LP/G395H	
3	4	CLEAR/PRISM F100LP/G140M F100LP/G140H F170LP/G235M F170LP/G235H F290LP/G395M F290LP/G395H	
4	1	CLEAR/PRISM F100LP/G140M F100LP/G140H F170LP/G235M F170LP/G235H F290LP/G395M F290LP/G395H	
5	2	CLEAR/PRISM F100LP/G140M F100LP/G140H F170LP/G235M F170LP/G235H F290LP/G395M F290LP/G395H	

Check with the JWST SOCCER Database at: <https://soccer.stsci.edu>
To verify that this is the current version.

5	3	CLEAR/PRISM	 <p>Observation 5:2 Position 5c (prism, Q3)</p>
6	4	CLEAR/PRISM	 <p>Observation 6 Position 6f (prism, Q4)</p>
7	1	CLEAR/PRISM	 <p>Observation 7 Position 7x (prism, Q1)</p>
8	2	CLEAR/PRISM	 <p>Observation 8 Position 8k (prism, Q2)</p>

To ensure the validity of our wavelength calibration check, we first verify that the source was well centered within the shutter for each observation. We detail this verification process in the next section.

Check with the JWST SOCCER Database at: <https://soccer.stsci.edu>
To verify that this is the current version.

3.1 Source Centering Verification

In this program, each observation took two diagnostic image types to verify source centering: TA_CONFIRM images, taken immediately after the MSATA centering slew, and MSA_CONFIRM images, acquired just after MSATA and after configuring the MSA shutters into a new open/closed slitlet pattern. To analyze both image types, we perform simulations with an algorithm that is similar to the procedure to assess the centering accuracy achieved by the MSATA during each observation. The algorithm utilizes a least square fitting routine to estimate the residual pointing errors—V2 offset, V3 offset, and roll offset—by comparing the measured star positions in the confirmation images to their expected locations from APT. These derived solutions are indicative of the centering accuracy in these images.

First, we applied the algorithm to the measured centroids of the TA reference stars in the TA_CONFIRM image. Since only a single image is taken in this case, typically 5–8 centroids are available for the least-squares fit. Although MSA bars may partially obscure some centroids, the available sampling of the point spread function (PSF) in the image is sufficient to allow for accurate centroiding despite these obstructions. Next, we apply the algorithm to the measured centroids of the science targets in the small number of open shutters in the MSA_CONFIRM image. In this case, the PSF sampling along the dispersion direction (x-coordinate) is more limited, since only 1×3 shutters are open, providing illumination over just ~ 3 pixels. However, the MSA_CONFIRM image generally benefits from having a larger number of targets, ranging from 23 to 129 in the 06642 visits, although some get rejected in certain visits.

To summarize, the results from the TA_CONFIRM and MSA_CONFIRM images are consistent with each other and generally 20 mas or better—the expected TA accuracy within which we expect to meet the performance requirements for flux and wavelength calibration—with typical image-derived pointing offsets ranging from 2 to 8 mas. We note that Observation 5 shows slightly higher offsets from 10 to 13 mas, and Observation 3 exhibits a notably larger offset in the MSA_CONFIRM image (20 mas) compared to the TA_CONFIRM image (2 mas). Table 3.2 summarizes these results, listing the V2, V3, and roll offsets (all in arcseconds), the number of measurements used in each fit (e.g., "7 of 8" reference stars), and the differences between measured and expected centroid positions in the science coordinate frame's X (dispersion) and Y (cross-dispersion) directions for the target (sourceID 4210 in this program), expressed in pixels. Offsets from the center in the dispersion direction would shift the spectrum's position on the detector and could present systematic errors in the wavelength assignments. For instance, if the target is off-center in the dispersion direction by 10 mas, that roughly translates to 0.1 pixels on the detector, i.e., about 1/20 of a resolution element (depending on the disperser). In Table 3.2, we report the dispersion-direction offsets as absolute fractions of a resolution element. We also note that these offsets are small and do not propagate through the pipeline, as it assumes the target is well centered in the aperture as planned.

Table 3.2: TA_CONFIRM and MSA_CONFIRM Centering Analysis Results

Observation ID	2:1	3:1	5:1	5:2	7:1	8:1
TA V2 Offset (arcsec)	0.0045	0.0011	0.0129	-0.0099	0.0015	0.0009
TA V3 Offset (arcsec)	-0.0020	0.0021	0.0021	-0.0021	0.0032	0.0017
TA Roll Offset (arcsec)	3.6544	15.7096	9.1493	23.3546	-12.6067	-7.8113
TA Targets Used	7 of 8	8 of 8	8 of 8	8 of 8	8 of 8	6 of 8
MSA V2 Offset (arcsec)	-0.0020	0.0196	0.0105	-0.0135	-0.0039	-0.0024
MSA V3 Offset (arcsec)	-0.0049	0.0018	-0.0040	0.0021	0.0016	-0.0011
MSA Roll Offset (arcsec)	17.6861	40.6990	1.5373	15.6028	3.9121	6.7370
MSA Targets Used	23 of 27	31 of 36	42 of 53	129 of 158	55 of 74	76 of 105
X_SCI_diff [†] (pixels)	-0.0454	-0.0925	-0.0341	0.0500	0.0193	0.0466
X_SCI_diff [†] (absolute fraction of a resolution element)	2.27%	4.63%	1.70%	2.50%	0.97%	2.33%
Y_SCI_diff [†] (pixels)	-0.0748	-0.1549	-0.0398	0.1203	0.0555	0.0165

[†] X is the dispersion direction; Y is the cross-dispersion direction. For X, the absolute fraction of a resolution element is computed assuming a resolution element size of 2 pixels.

4 Analysis

4.1 Pipeline Processing

We processed the data through Stages 1–3 of the JWST Calibration Pipeline version 1.18.0, using reference and parameter files from the CRDS context *1364.pmap*. All pipeline steps use default parameters unless otherwise specified.

First, we ran the uncalibrated (*_uncal*) FITS files through the Stage 1 Detector Processing pipeline (*calwebb_detector1*), adjusting the *jump* step's *expand_factor* to 3 to better flag large cosmic ray events (snowballs). We then ran the resulting countrate (*_rate*) FITS products through the Stage 2 Spectroscopic Processing pipeline (*calwebb_spec2*), using association (ASN) files to distinguish between science and background exposures and enable pixel-to-pixel background subtraction. Stage 2 is also the stage in which the GWA tilt gets accounted for. To correct for 1/f noise in the calibrated products, we additionally applied the NSClean step (*nsclean*) in *calwebb_spec2* using *fit_method* 'fft', with a sigma-clipped mask constructed using a *nsigma* value of 1.5 and setting *fit_histogram* to True and *mask_spectral_regions* to False. Finally, we ran the calibrated (*_cal*) FITS products through the Stage 3 Spectroscopic

Check with the JWST SOCCER Database at: <https://soccer.stsci.edu>
To verify that this is the current version.

Processing pipeline (*calwebb_spec3*) with pixel replacement (*pixel_replace*) set to True for filling in NaN (Not a Number) pixels. A representative set of Stage 3 2D and 1D spectral products is shown in Figure 4.1.

Section 4.2 details the analysis of these final spectral products.

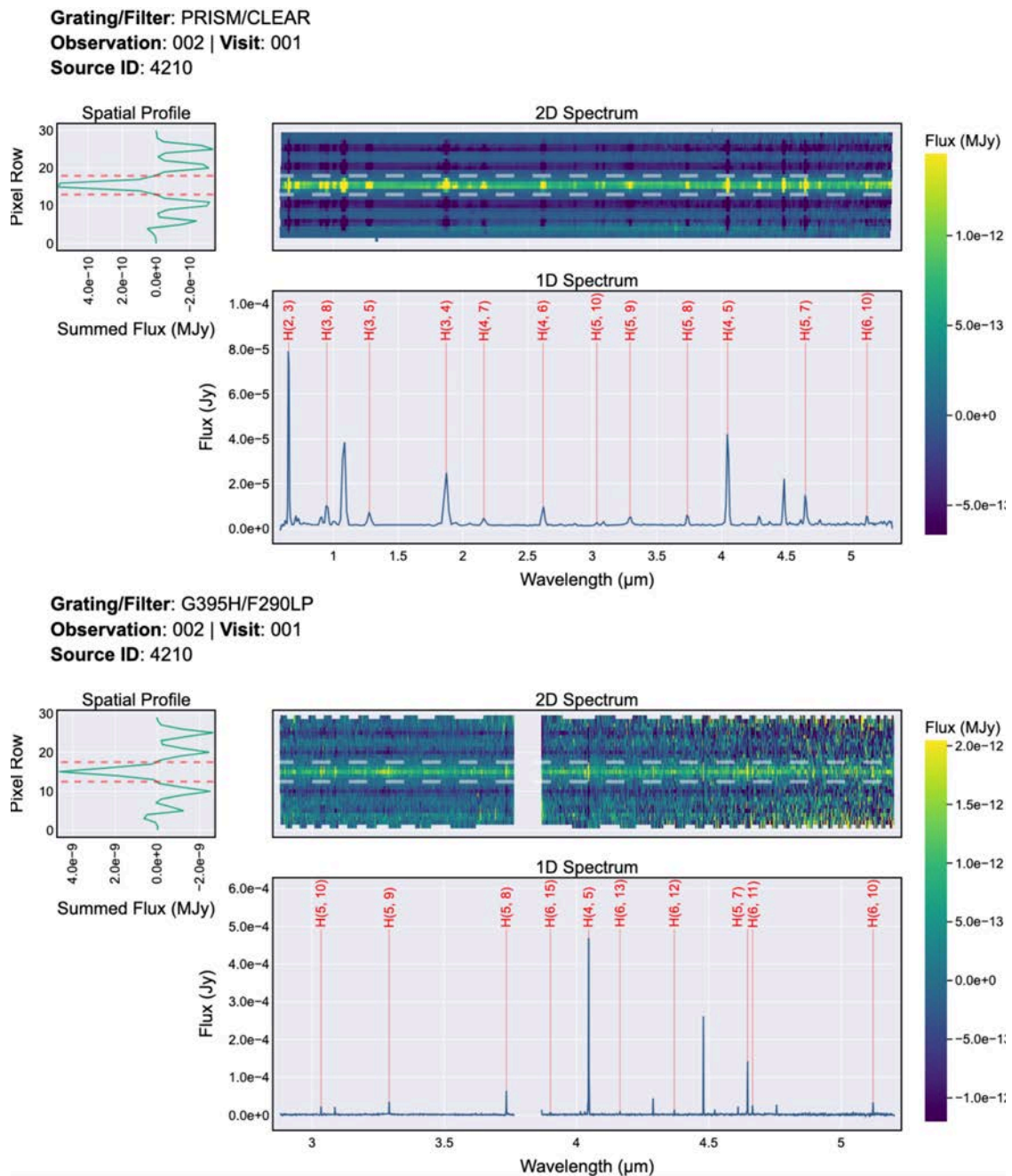


Figure 4.1: Representative, background subtracted Stage 3 2D and 1D spectral products. The top panels show spectra from the PRISM disperser, while the bottom panels display those from the G395H grating. In the G395H spectra, the wavelength gap between detectors is clearly visible. The 2D spectra are shown in the top rows, with the spatial profiles and 1D extraction regions highlighted in red/white. The bottom rows display the corresponding 1D spectra, with labeled hydrogen emission lines.

Check with the JWST SOCCER Database at: <https://soccer.stsci.edu>
 To verify that this is the current version.

4.2 Spectral Line Analysis

For this analysis, we primarily focused on fitting hydrogen recombination lines from the Balmer, Paschen, Brackett, Pfund, and Humphreys series, which together span the full NIRSpec wavelength range. We selected these lines based on the reasonable assumption that they share a common physical origin, thus having the same kinematics, allowing for a more accurate analysis of the wavelength calibration, without the potential introduction of outliers from higher-ionization lines that may probe different gas components. We identified these hydrogen lines using the Rydberg formula:

$$\frac{1}{\lambda} = R_H \left(\frac{1}{n_1^2} - \frac{1}{n_2^2} \right) \quad (2)$$

where λ is the wavelength, R_H is the Rydberg constant for hydrogen (calculated using *astropy.constants* as $1.0967758340280352 \times 10^7 \text{ m}^{-1}$), and n_1 and n_2 are the lower and upper principal quantum numbers, respectively. We validated these computed wavelengths by cross-referencing them with vacuum wavelengths from the *National Institute of Standards and Technology* (NIST) Atomic Spectra Database, finding good agreement to approximately seven significant digits (Kramida et al., 2024). This level of precision corresponds to a velocity accuracy of about $\pm 0.030 \text{ km/s}$ (see Equation 3) and an uncertainty in resolving power that is negligible compared to the uncertainty in the measured line width (see Equation 1). While not included in the primary analysis, the Appendix Table 7.1 contains results from fits to several non-hydrogen lines.

To accurately fit each emission line profile, we begin by estimating and subtracting the local continuum. We identify local continuum regions on either side of the line of interest and, assuming a generally flat local continuum, fit a constant value to these regions. In spectral regions with neighboring emission lines and noise spikes, we apply a 3-sigma clipping to reduce the influence of these nearby emission features on the continuum fit. To assess the impact of our continuum estimation on the line fit results, we derive three separate continuum levels using different percentile-based selection criteria (35th, 45th, 55th). As expected, the uncertainty in the exact value of the continuum level has a negligible impact on the line centroid position. Figure 4.2 shows a representative example for the Brackett γ (Bra_gamma) line, with the top panel comparing the three continuum levels/fits. In addition to fitting the continuum, we utilize these regions to estimate the line signal-to-noise ratio (SNR) and to help quantify measurement uncertainties, particularly for lines that may be harder to distinguish from the noise.

We applied two independent methods—empirical and parametric—to fit the spectral lines, to evaluate bias that would result from relying on a single approach. Figure 4.2 also shows a representative Brackett γ (Bra_gamma) line demonstrating both fitting methods. We performed the parametric fit using the Gaussian1D model from the *astropy* library, providing the laboratory wavelengths (as calculated in Eq. 2) as initial estimates for the central wavelength, along with initial estimates for the amplitude and width (from the observed spectrum). This method assumes a Gaussian line profile and iteratively adjusts the parameters to minimize the residuals between the observed flux and the model. The resulting Gaussian

Check with the JWST SOCCER Database at: <https://soccer.stsci.edu>
To verify that this is the current version.

model fit is plotted in red dashed lines in the middle panels of Figure 4.2. We also note that for the Gaussian model, we converted and report the resulting width as the full width at half maximum (FWHM). For the empirical method, we used the *centroid* and *gaussian_fwhm* functions from the *specutils* analysis library, applied to a sub-region of the spectrum centered on the line of interest, to estimate the central wavelength and FWHM. The *centroid* method uses the flux-weighted mean to determine the line center (first moment); while *gaussian_fwhm* uses second moment analysis to obtain the FWHM. These fit results are shown in the bottom panels of Figure 4.2. Both methods were applied to each line in every observation across all filter–grating combinations and later averaged for the results in Section 5.

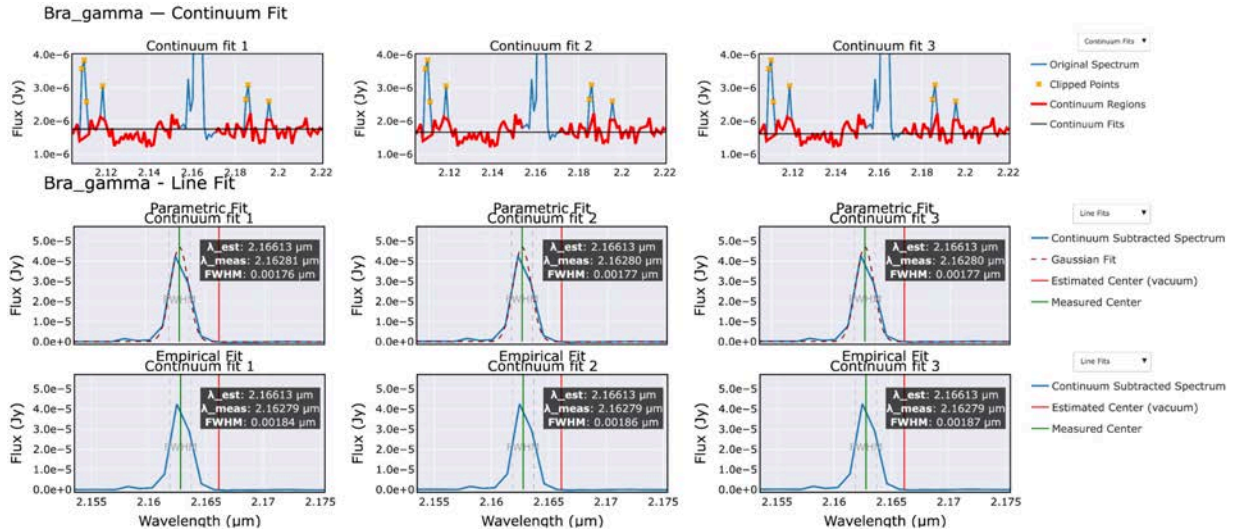


Figure 4.2: Continuum and emission line fitting procedure for a representative Brackett line observed with the G235M grating. Each column corresponds to a different assumed continuum level. *Top row:* Local continuum fits.

Bold red segments indicate the regions used to estimate the continuum (black line). The continuum panels are zoomed in to a narrow y-range to highlight the differences between continuum levels. To avoid contamination from nearby emission features, we apply 3σ clipping within these regions; clipped points are marked with orange crosses. *Middle row:* Parametric fit using a Gaussian1D model. The Gaussian profile (in dark red/brown) is plotted over the continuum-subtracted spectrum. *Bottom row:* Empirical fit using the *specutils* analysis library for centroid estimation. In the bottom two rows, the red vertical line marks the expected vacuum wavelength, the green line indicates the measured central wavelength of the emission feature, and the grey dashed lines denote the FWHM. Annotations display the numerical results for each fit.

In the next section, we detail how we used these resulting fits to validate the accuracy of the current wavelength calibration for NIRSpec's MOS mode as well as the resolving power.

5 Results

To quantify the wavelength calibration accuracy across the MSA FOV, we compute the offset between the measured central wavelength and the expected vacuum wavelength of each hydrogen emission line at each MSA position. These offsets are expressed in velocity units using the Doppler relation:

$$\Delta v = c \times \frac{\lambda_{obs} - \lambda_{vac}}{\lambda_{vac}} \quad (3)$$

where Δv is the velocity offset, c is the speed of light (299792.458 km/s from *astropy* constants), λ_{obs} is the observed central wavelength, and λ_{vac} is the known laboratory vacuum wavelength of the line (Kramida et al., 2024).

In Figure 5.1, we display two histograms showing the calculated velocity offsets for each line from each disperser, excluding the PRISM. Histograms for the medium- and high-resolution gratings are shown separately, with each grating/filter configuration color-coded. We exclude the PRISM from this analysis due to its low spectral resolution and correspondingly higher wavelength calibration uncertainty, which could bias the determination of the target's radial velocity. We also exclude lines with measured SNR < 20. Comparing the medium- and high-resolution grating averages of -452 ± 12 km/s and -458 ± 6 km/s, respectively, to the previously reported velocity of -445 ± 8 km/s for this target (SIMBAD; Kniazev et al., 2014), we find agreement within the uncertainties, although some disperser-dependent offsets/trends may be present, discussed more below. We use the overall average of -455 ± 10 km/s as the target radial velocity in this analysis.

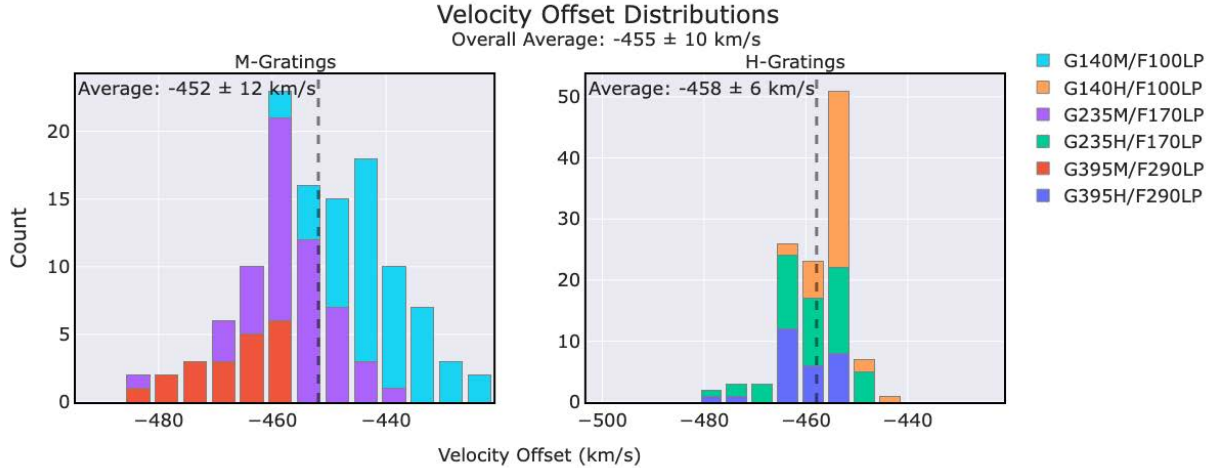


Figure 5.1: Velocity offset distributions for hydrogen emission lines measured with different NIRSpec grating-filter combinations. On the left is the M-grating and on the right the H-grating measurements. Each color highlights the offset distribution for a specific configuration, stacked for clarity. The histogram uses a small bin size. The black dashed lines indicate the average offset for each grating type, with the overall average annotated.

Overall, both line-fitting methods exhibit the same trends, so we report their average. A few lines show a larger spread with the empirical fit, but these are typically the lower-SNR cases. In Figures 5.2 through 5.4, we present the average velocity offsets and resolving powers (from both line-fitting methods) for each hydrogen line as a function of wavelength and MSA field position for the prism, medium-, and high-resolution gratings, respectively.

From Eq. 1, we calculated the resolving power using the measured centroid (λ) and FWHM ($\Delta\lambda$), with uncertainties derived by propagating their measurement errors. For a point source, we measure resolving powers that exceed expectations by $\sim 20\%$ overall, finding nominal resolving powers of ~ 170 for the PRISM, ~ 1200 for the medium-resolution gratings, and ~ 3000 for the high-resolution gratings. This improvement is primarily attributable to improved

OTE performance (much better wavefront error than the pre-launch requirement). Table 5.1 summarizes these results, together with the median ratio of measured to expected resolving power ($R_{\text{meas}}/R_{\text{exp}}$).

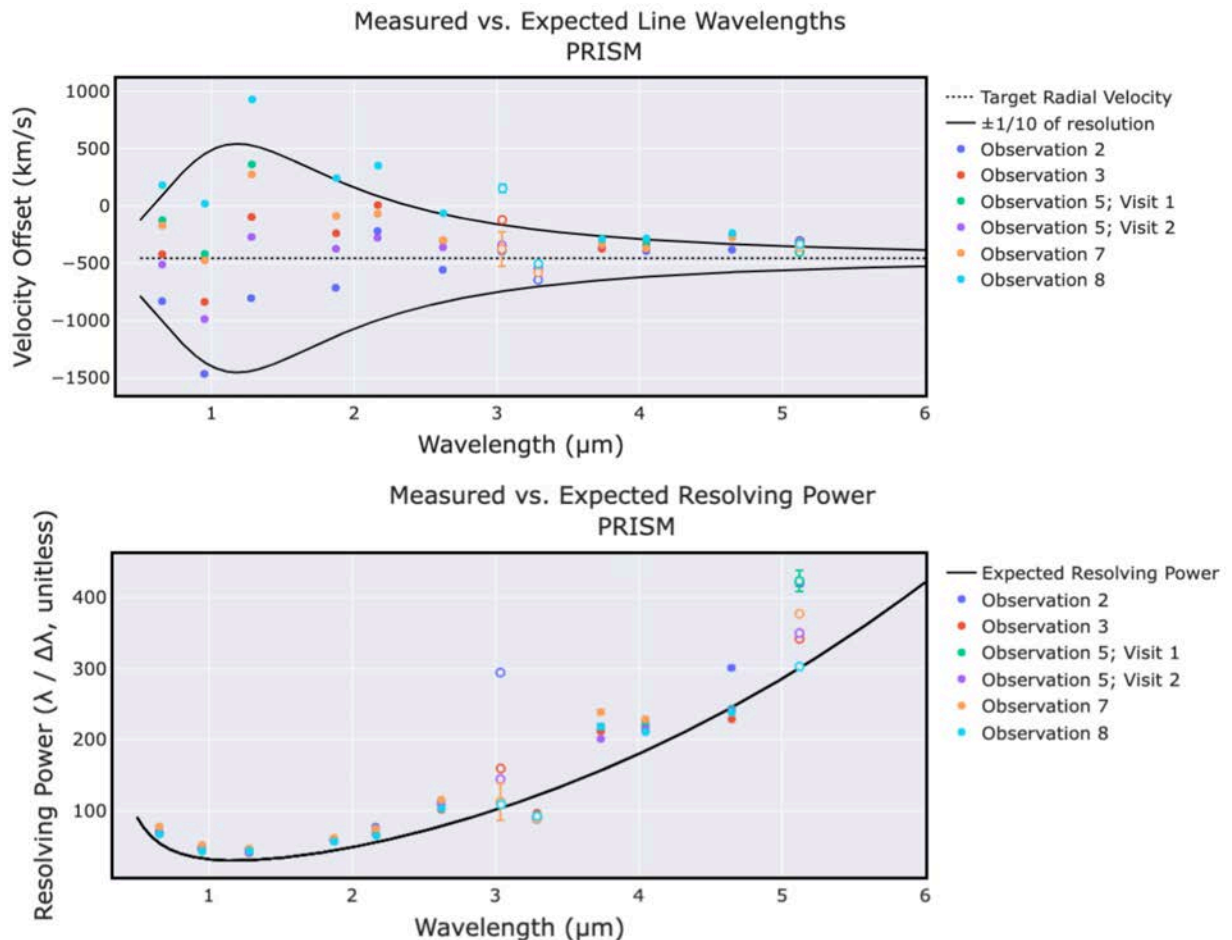


Figure 5.2: NIRSpec wavelength calibration and resolving power with the PRISM disperser. For both panels, each data point represents a hydrogen line and is the average of six measurements: two distinct line-fitting methods (empirical and parametric) combined with three different local continuum levels/fits. Solid circles represent data with a high SNR (>20), while open circles denote data with a lower SNR (<20). *Top Panel:* Displays the accuracy of the NIRSpec wavelength calibration, plotting the offsets between measured and expected line wavelengths, expressed in units of velocity (km/s). The dashed black line represents the radial velocity of the target we calculated in Figure 5.1. The solid black curves show $\pm 1/10$ resolution element, which represents NIRSpec’s internal wavelength calibration accuracy established during commissioning (Lützendorf et al., 2022). *Bottom Panel:* Displays the measured resolving power of each line compared to the expected values as a function of wavelength. Error bars in both plots show the standard error of the mean across the six measurements so most are small, larger bars reflect greater uncertainty in the continuum level estimate and/or the fit results.

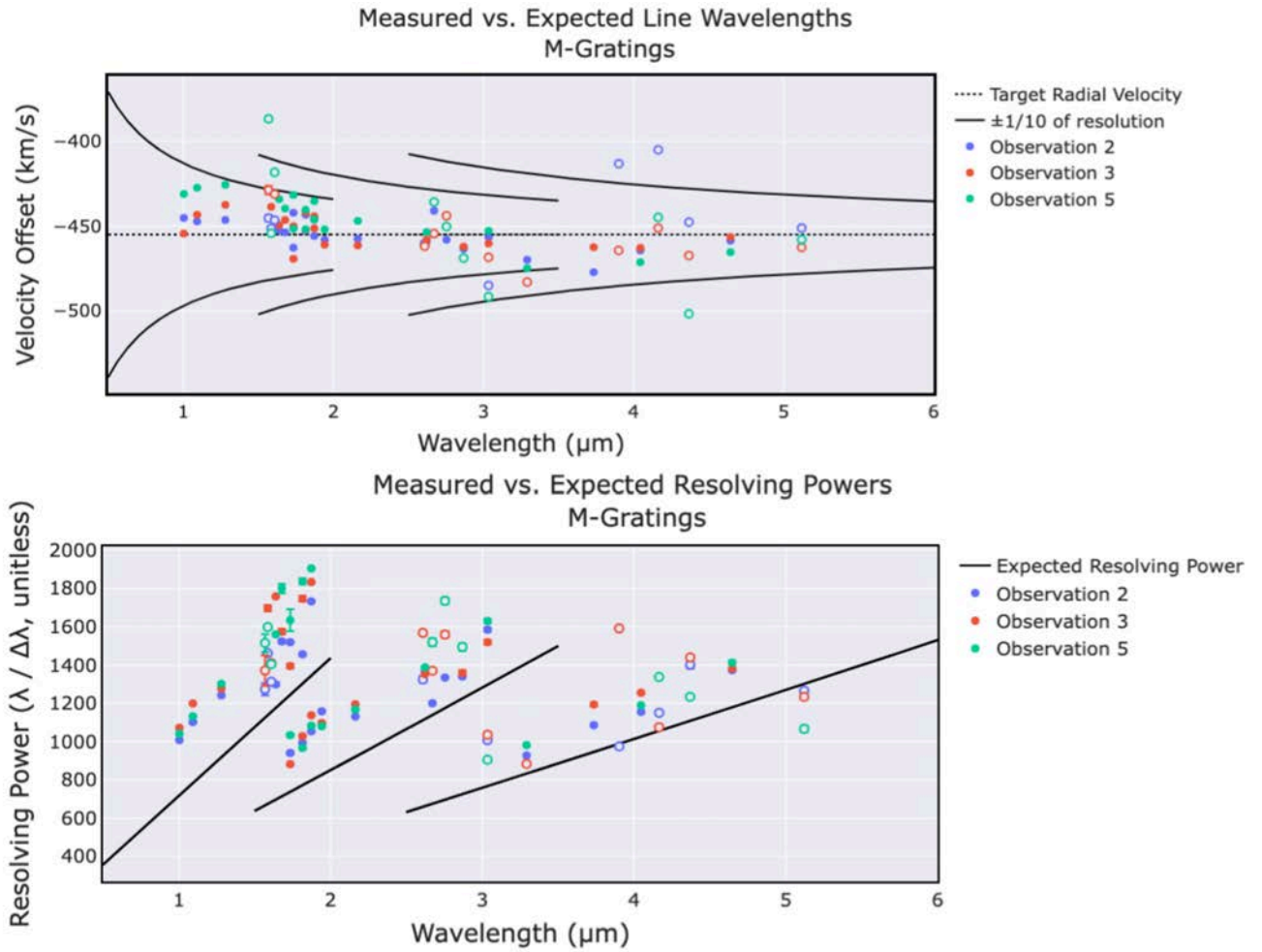


Figure 5.3: NIRSpec Wavelength Calibration and Resolving Power for All M-Gratings. This figure follows the same format as Figure 5.2, but displays the medium-resolution gratings (G140M, G235M, and G395M) from left to right. See Figure 5.2 for a detailed description of the panel contents.

Check with the JWST SOCCER Database at: <https://soccer.stsci.edu>
To verify that this is the current version.

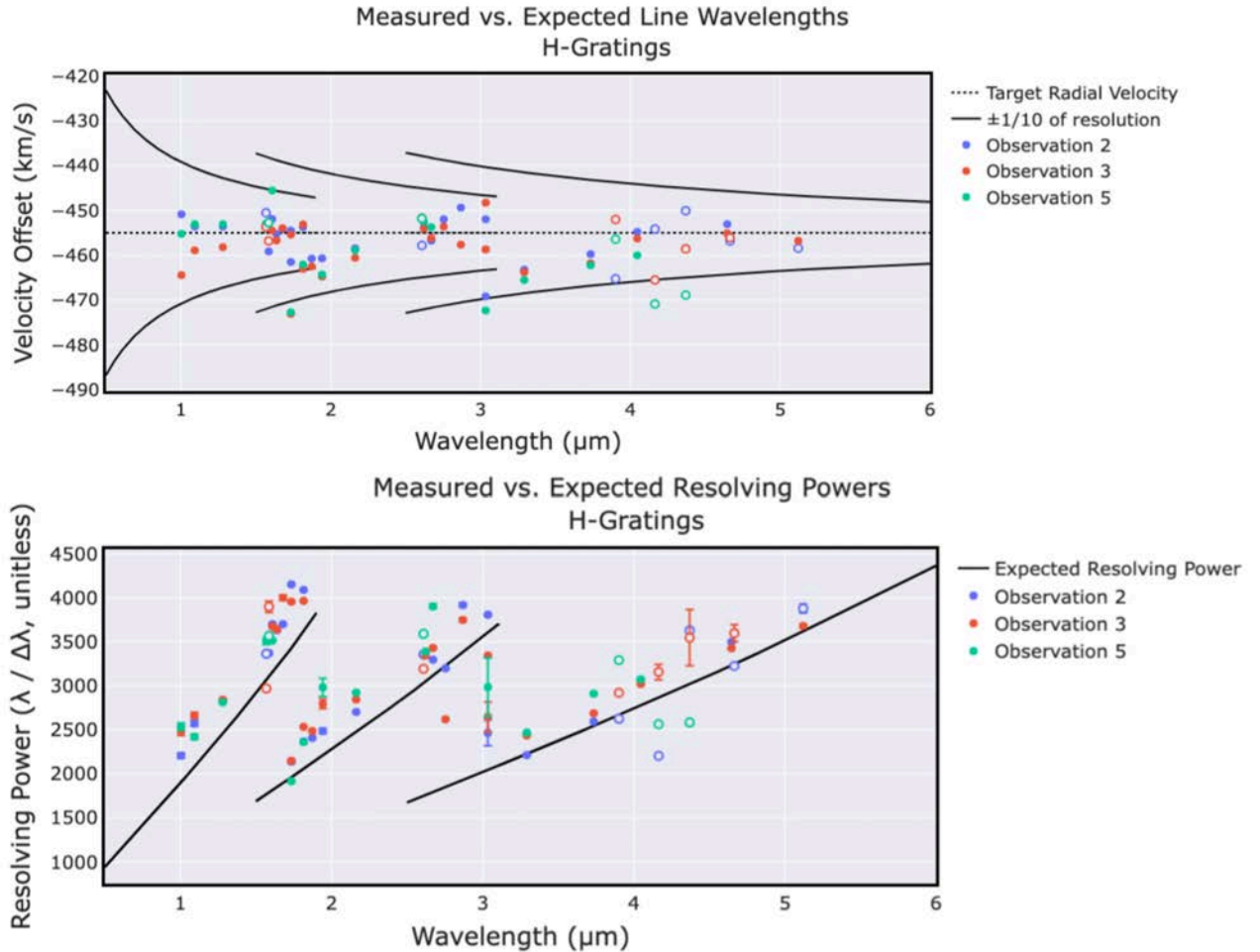


Figure 5.4: NIRSpec Wavelength Calibration and Resolving Power for All H-Gratings. This figure follows the same format as Figure 5.2, but displays the high-resolution gratings (G140H, G235H, and G395H) from left to right. See Figure 5.2 for a detailed description of the panel contents.

For the medium- and high-resolution gratings, most hydrogen line measurements fall within the $\pm 1/10$ of a resolution element boundaries, indicating that the wavelength calibration is within expected performance. Table 5.1 reports the actual measured range for each disperser. An expanded set of measured values is provided in Appendix Table 7.1. While we do remain within the required bounds, we do find lower-level trends/offsets in the data. In G140M, there appears to be a positive offset in the measurements. In both G395M, G395H, and G235H, there seems to be a linear trend: the measured velocities are lower than expected at the blue end of the range, and they approach the expected values towards the red. For most PRISM pointings, we find the wavelength calibration is within expected performance, except for one pointing (Observation 8, lower-right corner of Quadrant 2), which shows a systematic offset outside of these expected bounds. We also note that in some observations, a few lines are not fit because they fall within the detector wavelength gap. Additionally, in both the PRISM and the grating data, a few lines fall outside the boundaries, mostly low-SNR measurements that are more prone to fitting uncertainties.

Table 5.1: Wavelength Calibration and Resolving Power Summary

Disperser	Fraction of a Resolution Element [†]	Nominal R	Median R _{meas} /R _{exp}
G140M	-1/30 to +1/10	1200	1.351
G235M	±1/20		1.263
G395M	-1/12 to +1/25		1.165
G140H	±1/15	3000	1.153
G235H	±1/12		1.112
G395H	-1/10 to +1/25		1.093
PRISM	-1/15 to +1/10	170	1.298

[†] The fraction of a resolution element range does exclude some low SNR points.

6 Conclusions

Overall, this analysis demonstrates that for all filter-disperser configurations across the MSA field of view, the resolving powers are consistent with or exceed expectations, and the accuracy of the wavelength calibration generally fall within the quoted $\pm 1/10$ of a resolution element. The only exception is the PRISM configuration in Observation 8, which exhibits a systematic offset beyond the expected calibration bounds. The most probable explanations to explore are (i) a misplacement of the target in the dispersion direction or (ii) an error in the GWA tilt calibration.

Although this program sampled only a limited number of pointings across the MSA, we targeted the extreme corners of the FOV, so all other positions should fall within the measured range, as any residual distortions not captured by the instrument model should be a smooth function across the FOV. To confirm this, we are planning follow-up observations of the same planetary nebula in M31 in Cycle 4 at additional MSA field positions, using both the PRISM and gratings. These follow-up observations will also repeat the problematic MSA position in PRISM (Observation 8), as well as the missed MSA positions affected by the failed target acquisition in Observation 4 and the closed shutter in Observation 6.

7 Appendix

In the Appendix, we present figures in the same style as Figures 5.2–5.4 and a complete Table of results, using an extended line list that includes several non-hydrogen lines. The kinematic origin of these lines is more uncertain, and many are clear outliers relative to the hydrogen series. We include them here for completeness. In Table 7.1, we report the laboratory (vacuum) wavelength, measured wavelength, measured FWHM, velocity offset, and resolving power (R) for each line, disperser, and observation. Also note that in Table 7.1, we list the average of six measurements per line: two distinct line-fitting methods (empirical and parametric) combined with three different local continuum fits/levels. As expected, variations in the adopted continuum level have a negligible impact on the line measurements, so the resulting uncertainties on the averaged values are small and defined as described in the caption of Figure 5.2. Lines with low SNR are highlighted in orange.

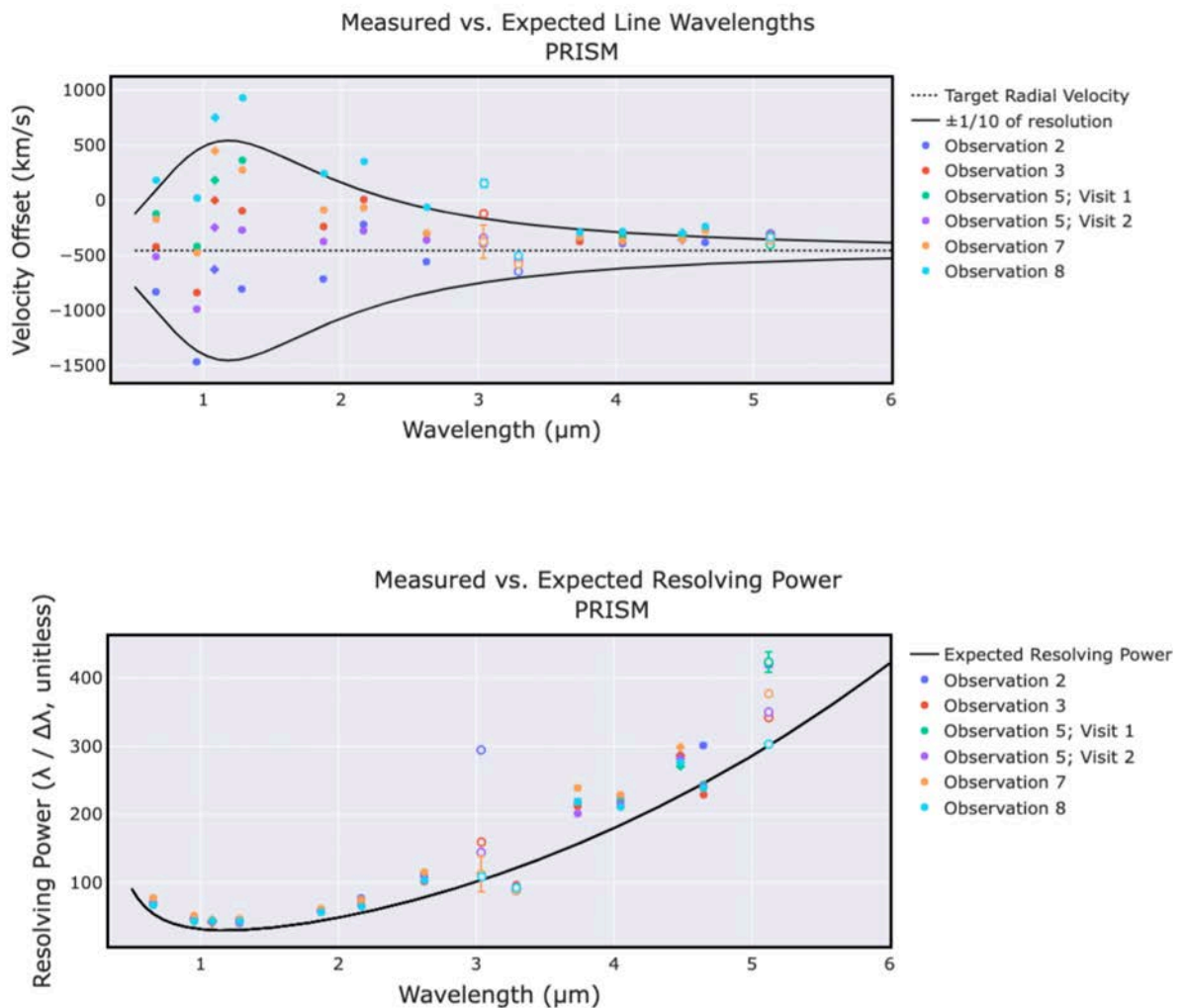


Figure 7.1: NIRSpec Wavelength Calibration and Resolving Power for PRISM disperser. This figure follows the same format as Figure 5.2 but with non-hydrogen lines included. See Figure 5.2 for a detailed description of each panel’s contents.

Check with the JWST SOCCER Database at: <https://soccer.stsci.edu>
To verify that this is the current version.

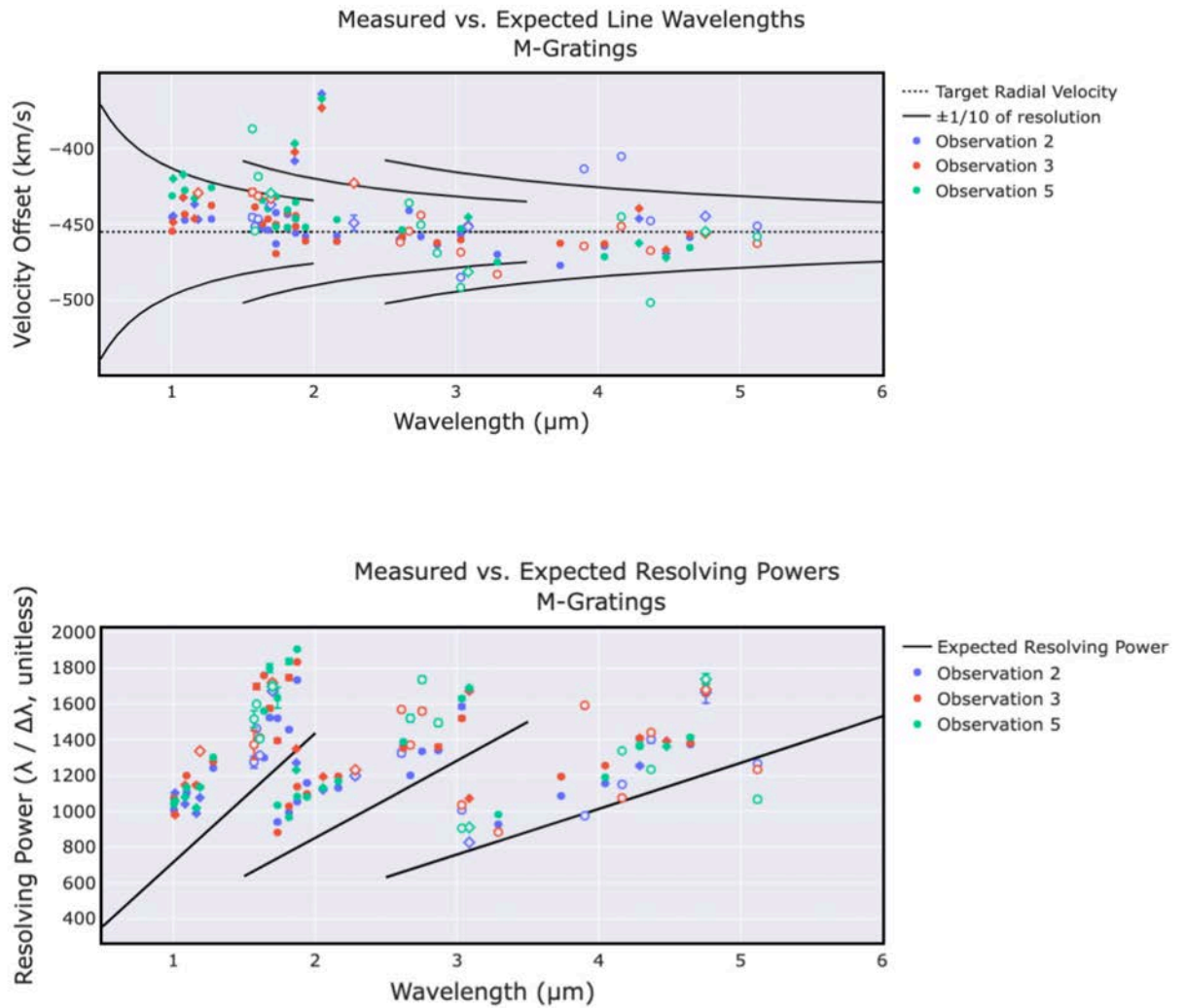


Figure 7.2: NIRSpec Wavelength Calibration and Resolving Power for All M-Gratings. This figure follows the same format as Figure 5.3 displaying the medium-resolution gratings (G140M, G235M, and G395M) from left to right but with non-hydrogen lines included. See Figure 5.2 for a detailed description of the panel contents.

Check with the JWST SOCCER Database at: <https://soccer.stsci.edu>
To verify that this is the current version.

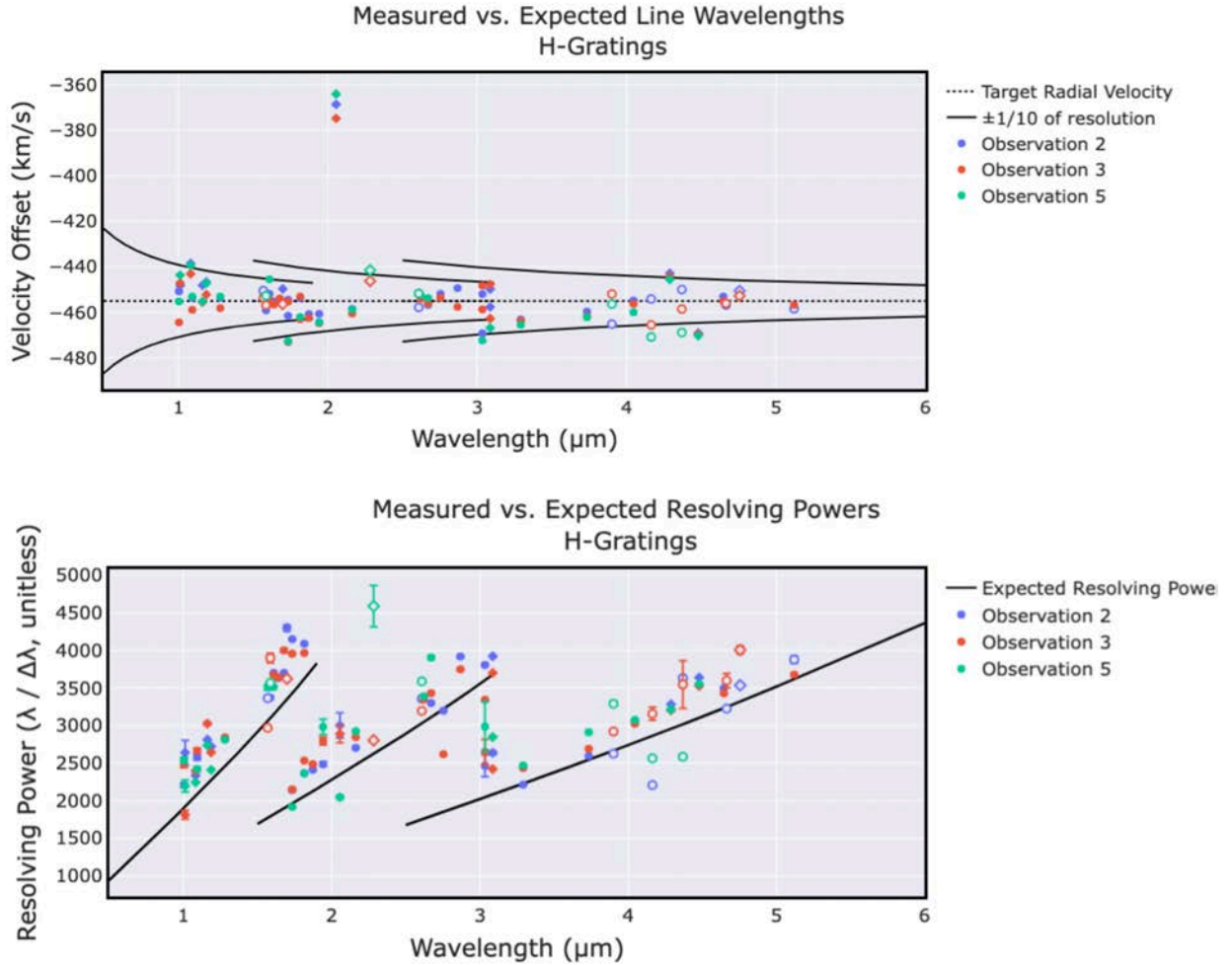


Figure 7.3: NIRSpec Wavelength Calibration and Resolving Power for All H-Gratings. This figure follows the same format as Figure 5.4, displaying the high-resolution gratings (G140H, G235H, and G395H) from left to right but with non-hydrogen lines included. See Figure 5.2 for a detailed description of the panel contents.

Table 7.1: Summary of Spectral Line Measurements by Disperser and Observation

Line	Lab λ (μm)	Grating	Obs.	Measured λ (μm)	Measured FWHM (μm)	Velocity Offset (km/s)	R
H α	0.6564696	PRISM	2:1	$0.6546563 \pm 1.14 \times 10^{-7}$	$(9.212 \pm 0.017) \times 10^{-3}$	-829.245 ± 0.052	71.06 ± 0.13
			3:1	$0.6555478 \pm 6.60 \times 10^{-8}$	$(9.697 \pm 0.006) \times 10^{-3}$	-421.261 ± 0.030	67.605 ± 0.040
			5:1	$0.6561972 \pm 5.08 \times 10^{-8}$	$(9.747 \pm 0.017) \times 10^{-3}$	-124.441 ± 0.023	67.32 ± 0.12
			5:2	$0.6553503 \pm 4.94 \times 10^{-7}$	$(9.355 \pm 0.011) \times 10^{-3}$	-511.60 ± 0.23	70.052 ± 0.080
			7:1	$0.6560947 \pm 2.58 \times 10^{-7}$	$(8.430 \pm 0.007) \times 10^{-3}$	-171.26 ± 0.12	77.830 ± 0.068
			8:1	$0.6568654 \pm 5.02 \times 10^{-7}$	$(9.824 \pm 0.017) \times 10^{-3}$	180.70 ± 0.23	66.86 ± 0.12
Pa ϵ	0.9548649	PRISM	2:1	$0.9502109 \pm 1.85 \times 10^{-5}$	$(1.964 \pm 0.008) \times 10^{-2}$	-1464.8 ± 5.8	48.39 ± 0.19
			3:1	$0.9522062 \pm 1.28 \times 10^{-5}$	$(2.117 \pm 0.006) \times 10^{-2}$	-835.9 ± 4.0	44.98 ± 0.13
			5:1	$0.9535328 \pm 2.06 \times 10^{-7}$	$(2.202 \pm 0.000) \times 10^{-2}$	-418.530 ± 0.065	43.3036 ± 0.0052
			5:2	$0.9517273 \pm 3.86 \times 10^{-6}$	$(2.031 \pm 0.001) \times 10^{-2}$	-986.7 ± 1.2	46.855 ± 0.033
			7:1	$0.9533541 \pm 9.66 \times 10^{-6}$	$(1.846 \pm 0.007) \times 10^{-2}$	-474.7 ± 3.0	51.65 ± 0.21
			8:1	$0.9549308 \pm 8.95 \times 10^{-7}$	$(2.195 \pm 0.001) \times 10^{-2}$	20.71 ± 0.28	43.508 ± 0.014
Pa δ	1.0052191	G140H	2:1	$1.0037085 \pm 6.01 \times 10^{-7}$	$(4.550 \pm 0.086) \times 10^{-4}$	-450.84 ± 0.18	2206 ± 42
			3:1	$1.0036629 \pm 7.69 \times 10^{-7}$	$(4.039 \pm 0.112) \times 10^{-4}$	-464.46 ± 0.23	2485 ± 69
			5:1	$1.0036939 \pm 4.60 \times 10^{-7}$	$(3.957 \pm 0.092) \times 10^{-4}$	-455.20 ± 0.14	2537 ± 59
		G140M	2:1	$1.0037274 \pm 2.16 \times 10^{-7}$	$(9.967 \pm 0.028) \times 10^{-4}$	-445.196 ± 0.065	1007.1 ± 2.9
			3:1	$1.0036963 \pm 2.51 \times 10^{-8}$	$(9.363 \pm 0.020) \times 10^{-4}$	-454.4821 ± 0.0075	1072.0 ± 2.3
			5:1	$1.0037747 \pm 7.25 \times 10^{-8}$	$(9.654 \pm 0.030) \times 10^{-4}$	-431.076 ± 0.022	1039.7 ± 3.2
HeII 10126	1.0126300	G140H	2:1	$1.0111168 \pm 8.18 \times 10^{-7}$	$(3.834 \pm 0.339) \times 10^{-4}$	-448.31 ± 0.24	2637 ± 233
			3:1	$1.0111208 \pm 1.14 \times 10^{-6}$	$(5.584 \pm 0.249) \times 10^{-4}$	-447.13 ± 0.34	1811 ± 81
			5:1	$1.0111324 \pm 9.99 \times 10^{-7}$	$(4.606 \pm 0.237) \times 10^{-4}$	-443.69 ± 0.30	2195 ± 113

Check with the JWST SOCCER Database at: <https://soccer.stsci.edu>
To verify that this is the current version.

Line	Lab λ (μm)	Grating	Obs.	Measured λ (μm)	Measured FWHM (μm)	Velocity Offset (km/s)	R
HeI 10833	1.0833250	G140M	2:1	$1.0111300 \pm 5.72 \times 10^{-8}$	$(9.174 \pm 0.051) \times 10^{-4}$	-444.410 \pm 0.017	1102.1 \pm 6.1
			3:1	$1.0111161 \pm 4.16 \times 10^{-7}$	$(1.032 \pm 0.012) \times 10^{-3}$	-448.52 \pm 0.12	980 \pm 12
			5:1	$1.0112133 \pm 3.60 \times 10^{-8}$	$(9.559 \pm 0.078) \times 10^{-4}$	-419.720 \pm 0.011	1057.8 \pm 8.7
		G140H	2:1	$1.0817413 \pm 8.91 \times 10^{-9}$	$(4.632 \pm 0.003) \times 10^{-4}$	-438.5805 \pm 0.0025	2335.6 \pm 1.7
			3:1	$1.0817250 \pm 1.12 \times 10^{-8}$	$(4.516 \pm 0.003) \times 10^{-4}$	-443.1088 \pm 0.0031	2395.4 \pm 1.8
			5:1	$1.0817384 \pm 8.72 \times 10^{-9}$	$(4.822 \pm 0.003) \times 10^{-4}$	-439.3738 \pm 0.0024	2243.2 \pm 1.5
		G140M	2:1	$1.0817642 \pm 2.41 \times 10^{-10}$	$(1.040 \pm 0.000) \times 10^{-3}$	-432.235793 \pm 0.000067	1040.52 \pm 0.12
			3:1	$1.0817648 \pm 7.25 \times 10^{-9}$	$(9.437 \pm 0.001) \times 10^{-4}$	-432.0834 \pm 0.0020	1146.26 \pm 0.17
			5:1	$1.0818193 \pm 2.36 \times 10^{-9}$	$(1.003 \pm 0.000) \times 10^{-3}$	-416.97155 \pm 0.00065	1078.345 \pm 0.098
PRISM	2:1	$1.0810608 \pm 4.84 \times 10^{-7}$	$(2.542 \pm 0.006) \times 10^{-2}$	-627.23 \pm 0.13	42.529 \pm 0.098		
	3:1	$1.0833229 \pm 3.13 \times 10^{-7}$	$(2.619 \pm 0.007) \times 10^{-2}$	-0.569 \pm 0.086	41.37 \pm 0.11		
	5:1	$1.0839834 \pm 1.33 \times 10^{-6}$	$(2.508 \pm 0.005) \times 10^{-2}$	182.14 \pm 0.37	43.221 \pm 0.088		
	5:2	$1.0824316 \pm 6.52 \times 10^{-7}$	$(2.485 \pm 0.004) \times 10^{-2}$	-247.35 \pm 0.18	43.563 \pm 0.077		
	7:1	$1.0849412 \pm 1.73 \times 10^{-6}$	$(2.355 \pm 0.004) \times 10^{-2}$	446.93 \pm 0.48	46.070 \pm 0.070		
G140M	8:1	$1.0860392 \pm 2.47 \times 10^{-6}$	$(2.478 \pm 0.011) \times 10^{-2}$	750.18 \pm 0.68	43.82 \pm 0.20		
	2:1	$1.0924617 \pm 1.07 \times 10^{-7}$	$(4.247 \pm 0.070) \times 10^{-4}$	-453.644 \pm 0.029	2572 \pm 42		
	3:1	$1.0924424 \pm 8.74 \times 10^{-8}$	$(4.099 \pm 0.072) \times 10^{-4}$	-458.932 \pm 0.024	2665 \pm 47		
G140M	5:1	$1.0924637 \pm 8.64 \times 10^{-8}$	$(4.515 \pm 0.075) \times 10^{-4}$	-453.088 \pm 0.024	2420 \pm 40		
	2:1	$1.0924849 \pm 6.03 \times 10^{-8}$	$(9.913 \pm 0.039) \times 10^{-4}$	-447.268 \pm 0.017	1102.0 \pm 4.4		
	3:1	$1.0924995 \pm 1.48 \times 10^{-9}$	$(9.117 \pm 0.011) \times 10^{-4}$	-443.24715 \pm 0.00041	1198.3 \pm 1.4		
G140H	5:1	$1.0925573 \pm 8.13 \times 10^{-8}$	$(9.654 \pm 0.017) \times 10^{-4}$	-427.390 \pm 0.022	1131.7 \pm 2.0		
	2:1	$1.1612228 \pm 2.48 \times 10^{-7}$	$(4.131 \pm 0.009) \times 10^{-4}$	-448.158 \pm 0.064	2811.3 \pm 6.2		
	3:1	$1.1611942 \pm 1.45 \times 10^{-8}$	$(3.838 \pm 0.036) \times 10^{-4}$	-455.5492 \pm 0.0037	3025 \pm 28		
G140H	5:1	$1.1611956 \pm 2.30 \times 10^{-7}$	$(4.241 \pm 0.012) \times 10^{-4}$	-455.183 \pm 0.059	2738.0 \pm 8.0		
	2:1	$1.1612674 \pm 3.17 \times 10^{-7}$	$(1.176 \pm 0.010) \times 10^{-3}$	-436.644 \pm 0.082	987.8 \pm 8.8		
	3:1	$1.1612303 \pm 4.70 \times 10^{-8}$	$(1.014 \pm 0.012) \times 10^{-3}$	-446.210 \pm 0.012	1145 \pm 13		
G140M	5:1	$1.1612824 \pm 5.13 \times 10^{-8}$	$(1.140 \pm 0.008) \times 10^{-3}$	-432.779 \pm 0.013	1018.6 \pm 6.7		
	2:1	$1.1868532 \pm 6.03 \times 10^{-7}$	$(4.361 \pm 0.017) \times 10^{-4}$	-446.70 \pm 0.15	2721 \pm 10		
	3:1	$1.1868315 \pm 6.73 \times 10^{-9}$	$(4.491 \pm 0.013) \times 10^{-4}$	-452.1817 \pm 0.0017	2642.4 \pm 7.8		
G140H	5:1	$1.1868512 \pm 1.22 \times 10^{-7}$	$(4.928 \pm 0.007) \times 10^{-4}$	-447.224 \pm 0.031	2408.6 \pm 3.5		
	2:1	$1.1868532 \pm 6.48 \times 10^{-7}$	$(1.103 \pm 0.005) \times 10^{-3}$	-446.72 \pm 0.16	1075.9 \pm 5.3		
	3:1	$1.1869226 \pm 7.67 \times 10^{-8}$	$(8.885 \pm 0.028) \times 10^{-4}$	-429.168 \pm 0.019	1335.9 \pm 4.2		
G140M	5:1	$1.1869200 \pm 2.14 \times 10^{-7}$	$(1.047 \pm 0.011) \times 10^{-3}$	-429.847 \pm 0.054	1134 \pm 12		
	2:1	$1.2802285 \pm 2.65 \times 10^{-9}$	$(4.537 \pm 0.022) \times 10^{-4}$	-453.63991 \pm 0.00062	2822 \pm 13		
	3:1	$1.2802089 \pm 1.52 \times 10^{-8}$	$(4.502 \pm 0.017) \times 10^{-4}$	-458.2274 \pm 0.0036	2844 \pm 11		
G140H	5:1	$1.2802310 \pm 9.99 \times 10^{-9}$	$(4.550 \pm 0.018) \times 10^{-4}$	-453.0620 \pm 0.0023	2813 \pm 11		
	2:1	$1.2802594 \pm 4.48 \times 10^{-8}$	$(1.032 \pm 0.001) \times 10^{-3}$	-446.405 \pm 0.010	1240.9 \pm 1.3		
	3:1	$1.2802977 \pm 3.12 \times 10^{-8}$	$(1.003 \pm 0.001) \times 10^{-3}$	-437.4489 \pm 0.0073	1276.4 \pm 1.4		
G140M	5:1	$1.2803484 \pm 5.83 \times 10^{-9}$	$(9.842 \pm 0.005) \times 10^{-4}$	-425.5754 \pm 0.0014	1300.88 \pm 0.65		
	2:1	$1.2787326 \pm 2.37 \times 10^{-6}$	$(2.796 \pm 0.014) \times 10^{-2}$	-804.13 \pm 0.55	45.73 \pm 0.23		
	3:1	$1.2817585 \pm 9.06 \times 10^{-6}$	$(3.162 \pm 0.008) \times 10^{-2}$	-95.6 \pm 2.1	40.54 \pm 0.10		
PRISM	5:1	$1.2837174 \pm 2.54 \times 10^{-5}$	$(3.149 \pm 0.009) \times 10^{-2}$	362.2 \pm 5.9	40.77 \pm 0.12		
	5:2	$1.2810135 \pm 6.08 \times 10^{-5}$	$(3.109 \pm 0.021) \times 10^{-2}$	-270 \pm 14	41.21 \pm 0.28		
	7:1	$1.2833371 \pm 9.74 \times 10^{-7}$	$(2.721 \pm 0.016) \times 10^{-2}$	273.42 \pm 0.23	47.16 \pm 0.28		
	8:1	$1.2861432 \pm 8.15 \times 10^{-6}$	$(2.957 \pm 0.007) \times 10^{-2}$	928.2 \pm 1.9	43.49 \pm 0.11		
	G140H	2:1	$1.5681432 \pm 4.17 \times 10^{-7}$	$(4.662 \pm 0.018) \times 10^{-4}$	-450.511 \pm 0.080	3364 \pm 13	
3:1		$1.5681266 \pm 7.43 \times 10^{-7}$	$(5.282 \pm 0.038) \times 10^{-4}$	-453.67 \pm 0.14	2969 \pm 21		
5:1		$1.5681304 \pm 1.20 \times 10^{-6}$	$(4.470 \pm 0.073) \times 10^{-4}$	-452.94 \pm 0.23	3508 \pm 58		
G140M	2:1	$1.5681704 \pm 1.47 \times 10^{-5}$	$(1.231 \pm 0.044) \times 10^{-3}$	-445.3 \pm 2.8	1274 \pm 45		
	3:1	$1.5682571 \pm 1.89 \times 10^{-5}$	$(1.144 \pm 0.095) \times 10^{-3}$	-428.7 \pm 3.6	1371 \pm 114		
	5:1	$1.5684767 \pm 9.03 \times 10^{-6}$	$(1.036 \pm 0.046) \times 10^{-3}$	-386.8 \pm 1.7	1515 \pm 67		
G140H	2:1	$1.5860635 \pm 1.50 \times 10^{-8}$	$(4.704 \pm 0.029) \times 10^{-4}$	-459.1177 \pm 0.0028	3372 \pm 21		
	3:1	$1.5860757 \pm 8.70 \times 10^{-8}$	$(4.069 \pm 0.096) \times 10^{-4}$	-456.822 \pm 0.016	3898 \pm 92		
	5:1	$1.5860971 \pm 5.00 \times 10^{-7}$	$(4.446 \pm 0.051) \times 10^{-4}$	-452.763 \pm 0.094	3568 \pm 41		
G140M	2:1	$1.5861045 \pm 5.35 \times 10^{-7}$	$(1.085 \pm 0.008) \times 10^{-3}$	-451.38 \pm 0.10	1462 \pm 10		
	3:1	$1.5861722 \pm 7.51 \times 10^{-7}$	$(9.349 \pm 0.128) \times 10^{-4}$	-438.58 \pm 0.14	1697 \pm 23		
	5:1	$1.5860889 \pm 1.42 \times 10^{-6}$	$(9.924 \pm 0.020) \times 10^{-4}$	-454.31 \pm 0.27	1598.2 \pm 3.3		
G140H	2:1	$1.6089508 \pm 1.03 \times 10^{-7}$	$(4.348 \pm 0.014) \times 10^{-4}$	-451.882 \pm 0.019	3700 \pm 12		
	3:1	$1.6089367 \pm 6.15 \times 10^{-8}$	$(4.380 \pm 0.014) \times 10^{-4}$	-454.517 \pm 0.011	3673 \pm 12		
	5:1	$1.6089848 \pm 1.14 \times 10^{-7}$	$(4.580 \pm 0.007) \times 10^{-4}$	-445.540 \pm 0.021	3513.2 \pm 5.7		
G140M	2:1	$1.6089799 \pm 8.02 \times 10^{-8}$	$(1.225 \pm 0.004) \times 10^{-3}$	-446.469 \pm 0.015	1312.9 \pm 4.7		
	3:1	$1.6090618 \pm 8.28 \times 10^{-7}$	$(1.141 \pm 0.013) \times 10^{-3}$	-431.20 \pm 0.15	1410 \pm 16		
	5:1	$1.6091312 \pm 1.43 \times 10^{-7}$	$(1.146 \pm 0.004) \times 10^{-3}$	-418.265 \pm 0.027	1404.4 \pm 5.1		
G140H	2:1	$1.6386835 \pm 2.57 \times 10^{-9}$	$(4.513 \pm 0.006) \times 10^{-4}$	-455.28040 \pm 0.00047	3630.8 \pm 4.7		
	3:1	$1.6386758 \pm 3.55 \times 10^{-8}$	$(4.501 \pm 0.006) \times 10^{-4}$	-456.7028 \pm 0.0065	3640.7 \pm 4.8		
	Wavelength Coverage Gap or No Fit						
G140M	2:1	$1.6386987 \pm 5.77 \times 10^{-7}$	$(1.261 \pm 0.010) \times 10^{-3}$	-452.50 \pm 0.11	1299 \pm 10		
	3:1	$1.6387151 \pm 4.23 \times 10^{-8}$	$(9.318 \pm 0.008) \times 10^{-4}$	-449.4998 \pm 0.0077	1758.6 \pm 1.5		
	5:1	$1.6387996 \pm 1.26 \times 10^{-7}$	$(1.050 \pm 0.000) \times 10^{-3}$	-434.054 \pm 0.023	1560.21 \pm 0.71		
G140H	2:1	$1.6785733 \pm 5.30 \times 10^{-8}$	$(4.536 \pm 0.010) \times 10^{-4}$	-454.1226 \pm 0.0095	3700.5 \pm 8.3		
	3:1	$1.6785742 \pm 5.01 \times 10^{-7}$	$(4.196 \pm 0.042) \times 10^{-4}$	-453.973 \pm 0.089	4000 \pm 40		
	Wavelength Coverage Gap or No Fit						

Check with the JWST SOCCER Database at: <https://soccer.stsci.edu>

To verify that this is the current version.

Line	Lab λ (μm)	Grating	Obs.	Measured λ (μm)	Measured FWHM (μm)	Velocity Offset (km/s)	R		
		G140M	2:1	$1.6785756 \pm 1.20 \times 10^{-6}$	$(1.102 \pm 0.009) \times 10^{-3}$	-453.71 ± 0.22	1523 ± 12		
			3:1	$1.6786163 \pm 1.80 \times 10^{-6}$	$(1.066 \pm 0.014) \times 10^{-3}$	-446.44 ± 0.32	1574 ± 21		
			5:1	$1.6786545 \pm 1.49 \times 10^{-7}$	$(9.328 \pm 0.179) \times 10^{-4}$	-439.620 ± 0.027	1800 ± 35		
HeI 17007	1.7007040	G140H	2:1	$1.6981548 \pm 3.17 \times 10^{-8}$	$(3.950 \pm 0.055) \times 10^{-4}$	-449.7059 ± 0.0056	4299 ± 60		
			3:1	$1.6981168 \pm 1.32 \times 10^{-8}$	$(4.688 \pm 0.010) \times 10^{-4}$	-456.4000 ± 0.0023	3622.6 ± 7.5		
		Wavelength Coverage Gap or No Fit							
		G140M	2:1	$1.6982273 \pm 2.23 \times 10^{-6}$	$(1.016 \pm 0.011) \times 10^{-3}$	-436.91 ± 0.39	1672 ± 18		
			3:1	$1.6982500 \pm 6.88 \times 10^{-7}$	$(9.891 \pm 0.138) \times 10^{-4}$	-432.90 ± 0.12	1717 ± 24		
			5:1	$1.6982704 \pm 4.10 \times 10^{-6}$	$(1.001 \pm 0.017) \times 10^{-3}$	-429.30 ± 0.72	1697 ± 28		
Bra 6	1.7366921	G140H	2:1	$1.7340613 \pm 1.22 \times 10^{-7}$	$(4.177 \pm 0.009) \times 10^{-4}$	-454.481 ± 0.021	4151.4 ± 8.5		
			3:1	$1.7340560 \pm 1.79 \times 10^{-7}$	$(4.385 \pm 0.010) \times 10^{-4}$	-455.387 ± 0.031	3954.5 ± 9.3		
			5:1	Wavelength Coverage Gap or No Fit					
		G140M	2:1	$1.7341323 \pm 8.96 \times 10^{-8}$	$(1.141 \pm 0.003) \times 10^{-3}$	-442.202 ± 0.015	1519.6 ± 4.1		
			3:1	$1.7340874 \pm 2.81 \times 10^{-6}$	$(1.244 \pm 0.014) \times 10^{-3}$	-449.97 ± 0.49	1394 ± 16		
			5:1	$1.7341933 \pm 7.94 \times 10^{-6}$	$(1.061 \pm 0.053) \times 10^{-3}$	-431.7 ± 1.4	1634 ± 82		
		G235H	2:1	$1.7340206 \pm 8.34 \times 10^{-7}$	$(8.103 \pm 0.091) \times 10^{-4}$	-461.52 ± 0.14	2140 ± 24		
			3:1	$1.7339536 \pm 9.32 \times 10^{-7}$	$(8.067 \pm 0.074) \times 10^{-4}$	-473.10 ± 0.16	2149 ± 20		
			5:1	$1.7339559 \pm 3.91 \times 10^{-7}$	$(9.051 \pm 0.062) \times 10^{-4}$	-472.700 ± 0.067	1916 ± 13		
		G235M	2:1	$1.7340132 \pm 1.42 \times 10^{-7}$	$(1.845 \pm 0.022) \times 10^{-3}$	-462.791 ± 0.025	940 ± 11		
			3:1	$1.7339750 \pm 1.90 \times 10^{-6}$	$(1.966 \pm 0.003) \times 10^{-3}$	-469.39 ± 0.33	882.0 ± 1.2		
			5:1	$1.7340781 \pm 1.85 \times 10^{-6}$	$(1.678 \pm 0.013) \times 10^{-3}$	-451.57 ± 0.32	1033.3 ± 8.3		
		Bra ϵ	1.8179158	G140H	2:1	$1.8151665 \pm 2.04 \times 10^{-8}$	$(4.440 \pm 0.013) \times 10^{-4}$	-453.7427 ± 0.0034	4088 ± 12
					3:1	$1.8151703 \pm 3.91 \times 10^{-8}$	$(4.578 \pm 0.004) \times 10^{-4}$	-453.1017 ± 0.0065	3965.3 ± 3.5
					5:1	Wavelength Coverage Gap or No Fit			
				G140M	2:1	$1.8152293 \pm 5.49 \times 10^{-7}$	$(1.246 \pm 0.007) \times 10^{-3}$	-443.369 ± 0.091	1456.6 ± 8.7
					3:1	$1.8152387 \pm 1.73 \times 10^{-6}$	$(1.039 \pm 0.012) \times 10^{-3}$	-441.82 ± 0.28	1747 ± 20
					5:1	$1.8152474 \pm 9.71 \times 10^{-7}$	$(9.881 \pm 0.121) \times 10^{-4}$	-440.37 ± 0.16	1837 ± 23
G235H	2:1			$1.8151120 \pm 3.26 \times 10^{-8}$	$(7.670 \pm 0.032) \times 10^{-4}$	-462.7405 ± 0.0054	2366.5 ± 10.0		
	3:1			$1.8151099 \pm 1.80 \times 10^{-7}$	$(7.165 \pm 0.017) \times 10^{-4}$	-463.085 ± 0.030	2533.3 ± 5.9		
	5:1			$1.8151160 \pm 2.93 \times 10^{-9}$	$(7.684 \pm 0.009) \times 10^{-4}$	-462.07260 ± 0.00048	2362.3 ± 2.8		
G235M	2:1			$1.8151732 \pm 1.10 \times 10^{-7}$	$(1.827 \pm 0.009) \times 10^{-3}$	-452.627 ± 0.018	993.6 ± 4.7		
	3:1			$1.8151764 \pm 4.71 \times 10^{-8}$	$(1.766 \pm 0.006) \times 10^{-3}$	-452.1065 ± 0.0078	1027.8 ± 3.6		
	5:1			$1.8151774 \pm 5.36 \times 10^{-7}$	$(1.880 \pm 0.004) \times 10^{-3}$	-451.933 ± 0.088	965.6 ± 1.9		
HeI 18690	1.8690000			G140M	2:1	$1.8664582 \pm 4.98 \times 10^{-7}$	$(1.469 \pm 0.000) \times 10^{-3}$	-407.987 ± 0.080	1270.66 ± 0.42
					3:1	$1.8664954 \pm 4.62 \times 10^{-7}$	$(1.384 \pm 0.001) \times 10^{-3}$	-402.021 ± 0.074	1348.33 ± 0.67
					5:1	$1.8665305 \pm 5.10 \times 10^{-7}$	$(1.516 \pm 0.004) \times 10^{-3}$	-396.380 ± 0.082	1231.0 ± 3.6
Pa α	1.8756274	G140M	2:1	$1.8728373 \pm 2.12 \times 10^{-10}$	$(1.081 \pm 0.000) \times 10^{-3}$	-446.293591 ± 0.000034	1732.17 ± 0.50		
			3:1	$1.8728501 \pm 3.50 \times 10^{-9}$	$(1.021 \pm 0.000) \times 10^{-3}$	-444.24075 ± 0.00056	1834.15 ± 0.32		
			5:1	$1.8729067 \pm 8.27 \times 10^{-9}$	$(9.832 \pm 0.003) \times 10^{-4}$	-435.1937 ± 0.0013	1904.96 ± 0.54		
		G235H	2:1	$1.8727470 \pm 3.09 \times 10^{-8}$	$(7.774 \pm 0.021) \times 10^{-4}$	-460.7535 ± 0.0049	2408.9 ± 6.6		
			3:1	$1.8727362 \pm 1.15 \times 10^{-8}$	$(7.531 \pm 0.015) \times 10^{-4}$	-462.4827 ± 0.0018	2486.7 ± 5.1		
			5:1	Wavelength Coverage Gap or No Fit					
		G235M	2:1	$1.8727779 \pm 1.02 \times 10^{-8}$	$(1.778 \pm 0.000) \times 10^{-3}$	-455.8048 ± 0.0016	1053.19 ± 0.28		
			3:1	$1.8728059 \pm 6.12 \times 10^{-9}$	$(1.646 \pm 0.000) \times 10^{-3}$	-451.32455 ± 0.00098	1137.56 ± 0.16		
			5:1	$1.8728383 \pm 1.01 \times 10^{-8}$	$(1.729 \pm 0.000) \times 10^{-3}$	-446.1372 ± 0.0016	1083.04 ± 0.11		
			PRISM	2:1	$1.8711633 \pm 1.17 \times 10^{-6}$	$(3.133 \pm 0.002) \times 10^{-2}$	-714.38 ± 0.19	59.726 ± 0.040	
				3:1	$1.8741361 \pm 3.14 \times 10^{-6}$	$(3.289 \pm 0.002) \times 10^{-2}$	-238.47 ± 0.50	56.977 ± 0.031	
				5:1	Wavelength Coverage Gap or No Fit				
		5:2	$1.8732867 \pm 1.21 \times 10^{-5}$	$(3.262 \pm 0.005) \times 10^{-2}$	-374.4 ± 1.9	57.436 ± 0.087			
		7:1	$1.8750759 \pm 7.60 \times 10^{-6}$	$(3.026 \pm 0.004) \times 10^{-2}$	-88.2 ± 1.2	61.969 ± 0.084			
		8:1	$1.8771415 \pm 2.68 \times 10^{-5}$	$(3.309 \pm 0.003) \times 10^{-2}$	241.9 ± 4.3	56.723 ± 0.047			
Bra δ	1.9450951	G235H	2:1	$1.9421085 \pm 1.74 \times 10^{-6}$	$(7.812 \pm 0.134) \times 10^{-4}$	-460.68 ± 0.27	2486 ± 43		
			3:1	$1.9420819 \pm 1.87 \times 10^{-6}$	$(6.949 \pm 0.185) \times 10^{-4}$	-464.79 ± 0.29	2795 ± 75		
			5:1	$1.9420849 \pm 2.69 \times 10^{-6}$	$(6.512 \pm 0.318) \times 10^{-4}$	-464.32 ± 0.41	2982 ± 146		
		G235M	2:1	$1.9421254 \pm 1.46 \times 10^{-7}$	$(1.678 \pm 0.008) \times 10^{-3}$	-458.070 ± 0.022	1157.2 ± 5.4		
			3:1	$1.9421060 \pm 5.22 \times 10^{-9}$	$(1.773 \pm 0.009) \times 10^{-3}$	-461.05863 ± 0.00081	1095.7 ± 5.4		
			5:1	$1.9421653 \pm 1.09 \times 10^{-7}$	$(1.799 \pm 0.005) \times 10^{-3}$	-451.904 ± 0.017	1079.4 ± 3.2		
HeI 20581	2.0581000	G235H	2:1	$2.0555711 \pm 2.93 \times 10^{-6}$	$(6.849 \pm 0.539) \times 10^{-4}$	-368.60 ± 0.43	3001 ± 236		
			3:1	$2.0555287 \pm 2.32 \times 10^{-6}$	$(7.121 \pm 0.398) \times 10^{-4}$	-374.78 ± 0.34	2887 ± 161		
			5:1	$2.0556020 \pm 1.48 \times 10^{-6}$	$(1.005 \pm 0.019) \times 10^{-3}$	-364.09 ± 0.22	2045 ± 39		
		G235M	2:1	$2.0556057 \pm 3.94 \times 10^{-7}$	$(1.838 \pm 0.008) \times 10^{-3}$	-363.558 ± 0.057	1118.1 ± 5.0		
			3:1	$2.0555420 \pm 4.15 \times 10^{-7}$	$(1.723 \pm 0.013) \times 10^{-3}$	-372.844 ± 0.061	1192.9 ± 9.0		
			5:1	$2.0555839 \pm 7.64 \times 10^{-7}$	$(1.818 \pm 0.010) \times 10^{-3}$	-366.72 ± 0.11	1130.7 ± 6.4		
Bra γ	2.1661287	G235H	2:1	$2.1628184 \pm 2.55 \times 10^{-10}$	$(8.002 \pm 0.006) \times 10^{-4}$	-458.485050 ± 0.000035	2702.7 ± 2.1		
			3:1	$2.1628035 \pm 4.77 \times 10^{-8}$	$(7.599 \pm 0.003) \times 10^{-4}$	-460.5546 ± 0.0066	2846.2 ± 1.1		
			5:1	$2.1628158 \pm 6.90 \times 10^{-8}$	$(7.399 \pm 0.004) \times 10^{-4}$	-458.8589 ± 0.0096	2922.9 ± 1.5		
		G235M	2:1	$2.1628253 \pm 6.98 \times 10^{-8}$	$(1.912 \pm 0.005) \times 10^{-3}$	-457.5333 ± 0.0097	1131.0 ± 2.9		
			3:1	$2.1627977 \pm 3.14 \times 10^{-7}$	$(1.811 \pm 0.002) \times 10^{-3}$	-461.365 ± 0.043	1194.3 ± 1.3		
			5:1	$2.1629018 \pm 2.65 \times 10^{-7}$	$(1.853 \pm 0.004) \times 10^{-3}$	-446.927 ± 0.037	1167.1 ± 2.4		
		PRISM	2:1	$2.1645434 \pm 1.86 \times 10^{-5}$	$(2.791 \pm 0.025) \times 10^{-2}$	-219.5 ± 2.6	77.57 ± 0.70		
			3:1	$2.1661876 \pm 4.16 \times 10^{-7}$	$(3.238 \pm 0.009) \times 10^{-2}$	8.149 ± 0.058	66.91 ± 0.19		
			5:1	Wavelength Coverage Gap or No Fit					

Check with the JWST SOCCER Database at: <https://soccer.stsci.edu>
 To verify that this is the current version.

Line	Lab λ (μm)	Grating	Obs.	Measured λ (μm)	Measured FWHM (μm)	Velocity Offset (km/s)	R	
			5:2	$2.1641309 \pm 4.16 \times 10^{-5}$	$(2.943 \pm 0.064) \times 10^{-2}$	-276.6 ± 5.8	73.5 ± 1.6	
			7:1	$2.1656438 \pm 1.44 \times 10^{-5}$	$(2.894 \pm 0.013) \times 10^{-2}$	-67.1 ± 2.0	74.83 ± 0.33	
			8:1	$2.1686685 \pm 3.08 \times 10^{-5}$	$(3.340 \pm 0.014) \times 10^{-2}$	351.3 ± 4.3	64.93 ± 0.28	
[C] 22866	2.2866000	G235H	2:1	$2.2831988 \pm 8.22 \times 10^{-7}$	$(8.147 \pm 0.012) \times 10^{-4}$	-446.26 ± 0.11	2802.4 ± 4.0	
			3:1	$2.2832349 \pm 1.49 \times 10^{-7}$	$(4.976 \pm 0.423) \times 10^{-4}$	-441.519 ± 0.020	4589 ± 390	
			5:1	Wavelength Coverage Gap or No Fit				
		G235M	2:1	$2.2831775 \pm 5.54 \times 10^{-5}$	$(1.906 \pm 0.037) \times 10^{-3}$	-449.1 ± 7.3	1198 ± 23	
			3:1	$2.2833784 \pm 8.89 \times 10^{-7}$	$(1.855 \pm 0.003) \times 10^{-3}$	-422.68 ± 0.12	1231.2 ± 2.2	
			5:1	Wavelength Coverage Gap or No Fit				
Pf 9	2.6126552	G235H	2:1	$2.6086683 \pm 4.57 \times 10^{-7}$	$(7.772 \pm 0.029) \times 10^{-4}$	-457.831 ± 0.053	3356 ± 12	
			3:1	$2.6087212 \pm 5.24 \times 10^{-7}$	$(8.169 \pm 0.011) \times 10^{-4}$	-451.749 ± 0.060	3193.4 ± 4.4	
			5:1	$2.6087208 \pm 4.61 \times 10^{-7}$	$(7.268 \pm 0.061) \times 10^{-4}$	-451.797 ± 0.053	3589 ± 30	
		G235M	2:1	$2.6086472 \pm 7.72 \times 10^{-7}$	$(1.969 \pm 0.037) \times 10^{-3}$	-460.251 ± 0.089	1325 ± 25	
			3:1	$2.6086335 \pm 4.21 \times 10^{-7}$	$(1.664 \pm 0.018) \times 10^{-3}$	-461.834 ± 0.048	1568 ± 17	
			5:1	Wavelength Coverage Gap or No Fit				
Bra β	2.6258784	G235H	2:1	$2.6219076 \pm 2.93 \times 10^{-8}$	$(7.753 \pm 0.004) \times 10^{-4}$	-453.6878 ± 0.0034	3381.8 ± 1.8	
			3:1	$2.6219045 \pm 2.22 \times 10^{-8}$	$(7.839 \pm 0.004) \times 10^{-4}$	-454.0434 ± 0.0025	3344.7 ± 1.5	
			5:1	$2.6219184 \pm 6.67 \times 10^{-8}$	$(7.738 \pm 0.005) \times 10^{-4}$	-452.4538 ± 0.0076	3388.4 ± 2.1	
		G235M	2:1	$2.6218599 \pm 3.33 \times 10^{-7}$	$(1.918 \pm 0.002) \times 10^{-3}$	-459.139 ± 0.038	1366.8 ± 1.3	
			3:1	$2.6218708 \pm 2.47 \times 10^{-8}$	$(1.938 \pm 0.002) \times 10^{-3}$	-457.8973 ± 0.0028	1352.8 ± 1.2	
			5:1	$2.6219092 \pm 3.23 \times 10^{-7}$	$(1.889 \pm 0.003) \times 10^{-3}$	-453.498 ± 0.037	1388.0 ± 2.0	
		PRISM	2:1	$2.6210143 \pm 5.90 \times 10^{-6}$	$(2.333 \pm 0.012) \times 10^{-2}$	-555.84 ± 0.67	112.36 ± 0.58	
			3:1	$2.6232457 \pm 5.61 \times 10^{-6}$	$(2.581 \pm 0.004) \times 10^{-2}$	-300.73 ± 0.64	101.63 ± 0.16	
			5:1	Wavelength Coverage Gap or No Fit				
			5:2	$2.6227271 \pm 1.29 \times 10^{-5}$	$(2.425 \pm 0.008) \times 10^{-2}$	-360.0 ± 1.5	108.16 ± 0.34	
			7:1	$2.6232721 \pm 1.53 \times 10^{-6}$	$(2.269 \pm 0.008) \times 10^{-2}$	-297.70 ± 0.18	115.60 ± 0.41	
			8:1	$2.6253162 \pm 1.73 \times 10^{-6}$	$(2.539 \pm 0.007) \times 10^{-2}$	-64.20 ± 0.20	103.40 ± 0.29	
Pf 8	2.6751390	G235H	2:1	$2.6710663 \pm 7.29 \times 10^{-7}$	$(8.100 \pm 0.007) \times 10^{-4}$	-456.759 ± 0.082	3297.5 ± 2.9	
			3:1	$2.6710717 \pm 2.30 \times 10^{-7}$	$(7.786 \pm 0.026) \times 10^{-4}$	-456.154 ± 0.026	3431 ± 11	
			5:1	$2.6710931 \pm 8.99 \times 10^{-7}$	$(6.843 \pm 0.064) \times 10^{-4}$	-453.74 ± 0.10	3903 ± 36	
		G235M	2:1	$2.6712076 \pm 6.25 \times 10^{-8}$	$(2.225 \pm 0.012) \times 10^{-3}$	-440.8949 ± 0.0070	1200.8 ± 6.3	
			3:1	$2.6710866 \pm 2.14 \times 10^{-7}$	$(1.949 \pm 0.030) \times 10^{-3}$	-454.473 ± 0.024	1370 ± 21	
			5:1	$2.6712527 \pm 4.76 \times 10^{-6}$	$(1.759 \pm 0.034) \times 10^{-3}$	-435.84 ± 0.53	1519 ± 29	
Pf 7	2.7582757	G235H	2:1	$2.7541207 \pm 2.10 \times 10^{-7}$	$(8.614 \pm 0.025) \times 10^{-4}$	-451.940 ± 0.023	3197.4 ± 9.1	
			3:1	$2.7541052 \pm 3.24 \times 10^{-7}$	$(1.052 \pm 0.000) \times 10^{-3}$	-453.621 ± 0.035	2618.83 ± 0.26	
			5:1	Wavelength Coverage Gap or No Fit				
		G235M	2:1	$2.7540643 \pm 1.24 \times 10^{-6}$	$(2.063 \pm 0.005) \times 10^{-3}$	-458.07 ± 0.13	1334.7 ± 3.0	
			3:1	$2.7541941 \pm 3.62 \times 10^{-7}$	$(1.766 \pm 0.027) \times 10^{-3}$	-443.944 ± 0.039	1559 ± 24	
			5:1	$2.7541357 \pm 3.75 \times 10^{-7}$	$(1.587 \pm 0.023) \times 10^{-3}$	-450.306 ± 0.041	1736 ± 25	
Pf 6	2.8730043	G235H	2:1	$2.8687010 \pm 4.91 \times 10^{-7}$	$(7.322 \pm 0.049) \times 10^{-4}$	-449.372 ± 0.051	3918 ± 26	
			3:1	$2.8686219 \pm 2.55 \times 10^{-8}$	$(7.653 \pm 0.050) \times 10^{-4}$	-457.6429 ± 0.0027	3748 ± 25	
			5:1	Wavelength Coverage Gap or No Fit				
		G235M	2:1	$2.8685655 \pm 5.97 \times 10^{-7}$	$(2.141 \pm 0.012) \times 10^{-3}$	-463.535 ± 0.062	1340.0 ± 7.5	
			3:1	$2.8685791 \pm 2.15 \times 10^{-6}$	$(2.110 \pm 0.028) \times 10^{-3}$	-462.12 ± 0.22	1360 ± 18	
			5:1	$2.8685140 \pm 1.04 \times 10^{-6}$	$(1.920 \pm 0.034) \times 10^{-3}$	-468.92 ± 0.11	1494 ± 26	
Pf ϵ	3.0392111	G235H	2:1	$3.0346325 \pm 5.92 \times 10^{-8}$	$(7.973 \pm 0.035) \times 10^{-4}$	-451.9855 ± 0.0058	3806 ± 17	
			3:1	$3.0346702 \pm 4.69 \times 10^{-7}$	$(9.074 \pm 0.013) \times 10^{-4}$	-448.258 ± 0.046	3344.2 ± 4.9	
			5:1	Wavelength Coverage Gap or No Fit				
		G235M	2:1	$3.0345857 \pm 1.52 \times 10^{-7}$	$(1.914 \pm 0.016) \times 10^{-3}$	-456.604 ± 0.015	1585 ± 13	
			3:1	$3.0345486 \pm 2.51 \times 10^{-6}$	$(1.997 \pm 0.021) \times 10^{-3}$	-460.27 ± 0.25	1519 ± 16	
			5:1	$3.0346242 \pm 5.09 \times 10^{-7}$	$(1.862 \pm 0.018) \times 10^{-3}$	-452.800 ± 0.050	1630 ± 16	
		G395H	2:1	$3.0344581 \pm 8.19 \times 10^{-7}$	$(1.231 \pm 0.103) \times 10^{-3}$	-469.209 ± 0.081	2465 ± 207	
			3:1	$3.0345647 \pm 4.94 \times 10^{-6}$	$(1.146 \pm 0.104) \times 10^{-3}$	-458.69 ± 0.49	2648 ± 240	
			5:1	$3.0344264 \pm 1.80 \times 10^{-6}$	$(1.016 \pm 0.160) \times 10^{-3}$	-472.35 ± 0.18	2986 ± 470	
		G395M	2:1	$3.0342977 \pm 3.20 \times 10^{-7}$	$(3.014 \pm 0.035) \times 10^{-3}$	-485.065 ± 0.032	1007 ± 12	
			3:1	$3.0344656 \pm 2.29 \times 10^{-6}$	$(2.932 \pm 0.056) \times 10^{-3}$	-468.47 ± 0.23	1035 ± 20	
			5:1	$3.0342298 \pm 2.68 \times 10^{-6}$	$(3.355 \pm 0.052) \times 10^{-3}$	-491.77 ± 0.26	904 ± 14	
			PRISM	2:1	$3.0352619 \pm 5.59 \times 10^{-5}$	$(1.031 \pm 0.122) \times 10^{-2}$	-389.8 ± 5.5	294 ± 35
				3:1	$3.0369577 \pm 6.90 \times 10^{-5}$	$(1.906 \pm 0.051) \times 10^{-2}$	-222.4 ± 6.8	159.3 ± 4.3
				5:1	Wavelength Coverage Gap or No Fit			
		5:2	$3.0357525 \pm 1.14 \times 10^{-5}$	$(2.102 \pm 0.010) \times 10^{-2}$	-341.4 ± 1.1	144.45 ± 0.68		
		7:1	$3.0354004 \pm 2.16 \times 10^{-3}$	$(2.691 \pm 0.881) \times 10^{-2}$	-376 ± 214	113 ± 37		
		8:1	$3.0407613 \pm 5.29 \times 10^{-4}$	$(2.792 \pm 2.306) \times 10^{-2}$	153 ± 52	109 ± 90		
HeII 30917	3.0916927	G235H	2:1	$3.0870572 \pm 4.21 \times 10^{-7}$	$(7.870 \pm 0.036) \times 10^{-4}$	-449.825 ± 0.041	3923 ± 18	
			3:1	$3.0870783 \pm 4.50 \times 10^{-7}$	$(8.343 \pm 0.022) \times 10^{-4}$	-447.775 ± 0.044	3700.2 ± 9.9	
			5:1	Wavelength Coverage Gap or No Fit				
		G235M	2:1	$3.0870539 \pm 2.80 \times 10^{-7}$	$(1.848 \pm 0.008) \times 10^{-3}$	-450.151 ± 0.027	1670.3 ± 6.8	
			3:1	$3.0870522 \pm 6.96 \times 10^{-7}$	$(1.845 \pm 0.010) \times 10^{-3}$	-450.318 ± 0.068	1672.8 ± 8.6	
			5:1	$3.0871049 \pm 1.09 \times 10^{-6}$	$(1.828 \pm 0.013) \times 10^{-3}$	-445.20 ± 0.11	1689 ± 12	
G395H	2:1	$3.0869764 \pm 1.59 \times 10^{-6}$	$(1.171 \pm 0.015) \times 10^{-3}$	-457.68 ± 0.15	2637 ± 34			

Check with the JWST SOCCER Database at: <https://soccer.stsci.edu>

To verify that this is the current version.

Line	Lab λ (μm)	Grating	Obs.	Measured λ (μm)	Measured FWHM (μm)	Velocity Offset (km/s)	R		
		G395M	3:1	$3.0869241 \pm 1.48 \times 10^{-6}$	$(1.275 \pm 0.004) \times 10^{-3}$	-462.75 ± 0.14	2421.1 ± 7.2		
			5:1	$3.0868819 \pm 3.12 \times 10^{-7}$	$(1.084 \pm 0.007) \times 10^{-3}$	-466.857 ± 0.030	2847 ± 18		
			2:1	$3.0870390 \pm 4.48 \times 10^{-7}$	$(3.740 \pm 0.016) \times 10^{-3}$	-451.600 ± 0.043	825.5 ± 3.5		
			3:1	$3.0867303 \pm 3.48 \times 10^{-6}$	$(2.880 \pm 0.008) \times 10^{-3}$	-481.58 ± 0.34	1071.6 ± 3.1		
			5:1	$3.0867313 \pm 9.88 \times 10^{-7}$	$(3.392 \pm 0.010) \times 10^{-3}$	-481.482 ± 0.096	910.0 ± 2.7		
Pf δ	3.2970014	G395H	2:1	$3.2919112 \pm 3.18 \times 10^{-7}$	$(1.488 \pm 0.002) \times 10^{-3}$	-463.203 ± 0.029	2211.9 ± 3.2		
			3:1	$3.2919050 \pm 5.63 \times 10^{-8}$	$(1.352 \pm 0.001) \times 10^{-3}$	-463.7679 ± 0.0051	2434.5 ± 2.2		
			5:1	$3.2918856 \pm 3.35 \times 10^{-7}$	$(1.334 \pm 0.001) \times 10^{-3}$	-465.532 ± 0.030	2467.3 ± 1.4		
		G395M	2:1	$3.2918379 \pm 2.13 \times 10^{-6}$	$(3.553 \pm 0.003) \times 10^{-3}$	-469.87 ± 0.19	926.62 ± 0.75		
			3:1	$3.2916935 \pm 5.17 \times 10^{-6}$	$(3.728 \pm 0.008) \times 10^{-3}$	-483.03 ± 0.47	883.1 ± 1.9		
			5:1	$3.2917821 \pm 2.61 \times 10^{-6}$	$(3.354 \pm 0.007) \times 10^{-3}$	-474.96 ± 0.24	981.5 ± 2.1		
		PRISM	2:1	$3.2899251 \pm 1.18 \times 10^{-4}$	$(3.717 \pm 0.057) \times 10^{-2}$	-644 ± 11	88.5 ± 1.4		
			3:1	$3.2910604 \pm 8.18 \times 10^{-5}$	$(3.390 \pm 0.035) \times 10^{-2}$	-540.7 ± 7.4	97.1 ± 1.0		
			5:1	Wavelength Coverage Gap or No Fit					
			5:2	$3.2910316 \pm 1.13 \times 10^{-4}$	$(3.613 \pm 0.038) \times 10^{-2}$	-543 ± 10	91.08 ± 0.97		
			7:1	$3.2906282 \pm 2.97 \times 10^{-4}$	$(3.704 \pm 0.085) \times 10^{-2}$	-580 ± 27	88.8 ± 2.0		
			8:1	$3.2914823 \pm 1.36 \times 10^{-4}$	$(3.555 \pm 0.083) \times 10^{-2}$	-502 ± 12	92.6 ± 2.2		
Pf γ	3.7405676	G395H	2:1	$3.7348358 \pm 8.34 \times 10^{-8}$	$(1.440 \pm 0.001) \times 10^{-3}$	-459.7297 ± 0.0067	2593.3 ± 2.5		
			3:1	$3.7348102 \pm 1.07 \times 10^{-7}$	$(1.389 \pm 0.002) \times 10^{-3}$	-461.7885 ± 0.0086	2689.3 ± 3.7		
			5:1	$3.7348049 \pm 2.92 \times 10^{-8}$	$(1.284 \pm 0.003) \times 10^{-3}$	-462.2131 ± 0.0023	2909.4 ± 5.9		
		G395M	2:1	$3.7346185 \pm 3.22 \times 10^{-6}$	$(3.443 \pm 0.006) \times 10^{-3}$	-477.18 ± 0.26	1084.8 ± 2.0		
			3:1	$3.7348013 \pm 4.01 \times 10^{-6}$	$(3.130 \pm 0.024) \times 10^{-3}$	-462.50 ± 0.32	1193.2 ± 9.3		
			5:1	Wavelength Coverage Gap or No Fit					
		PRISM	2:1	$3.7360201 \pm 6.90 \times 10^{-6}$	$(1.708 \pm 0.033) \times 10^{-2}$	-364.68 ± 0.55	218.7 ± 4.2		
			3:1	$3.7359028 \pm 6.45 \times 10^{-5}$	$(1.760 \pm 0.016) \times 10^{-2}$	-374.1 ± 5.2	212.2 ± 2.0		
			5:1	Wavelength Coverage Gap or No Fit					
			5:2	$3.7363378 \pm 1.42 \times 10^{-5}$	$(1.858 \pm 0.013) \times 10^{-2}$	-339.2 ± 1.1	201.1 ± 1.4		
			7:1	$3.7363785 \pm 1.30 \times 10^{-5}$	$(1.564 \pm 0.026) \times 10^{-2}$	-335.9 ± 1.0	239.0 ± 3.9		
			8:1	$3.7369607 \pm 6.09 \times 10^{-6}$	$(1.711 \pm 0.036) \times 10^{-2}$	-289.22 ± 0.49	218.4 ± 4.6		
Hu 9	3.9075572	G395H	2:1	$3.9014976 \pm 9.20 \times 10^{-7}$	$(1.486 \pm 0.000) \times 10^{-3}$	-465.257 ± 0.071	2624.731 ± 0.045		
			3:1	$3.9016698 \pm 1.10 \times 10^{-6}$	$(1.337 \pm 0.005) \times 10^{-3}$	-452.025 ± 0.085	2919 ± 12		
			5:1	$3.9016123 \pm 4.00 \times 10^{-8}$	$(1.186 \pm 0.008) \times 10^{-3}$	-456.4452 ± 0.0031	3290 ± 21		
		G395M	2:1	$3.9021755 \pm 3.95 \times 10^{-6}$	$(4.004 \pm 0.068) \times 10^{-3}$	-413.17 ± 0.30	974 ± 17		
			3:1	$3.9015093 \pm 4.85 \times 10^{-6}$	$(2.452 \pm 0.007) \times 10^{-3}$	-464.36 ± 0.37	1591.0 ± 4.2		
			5:1	Wavelength Coverage Gap or No Fit					
Bra α	4.0522815	G395H	2:1	$4.0461391 \pm 3.33 \times 10^{-9}$	$(1.320 \pm 0.000) \times 10^{-3}$	-454.76599 ± 0.00025	3064.6 ± 1.1		
			3:1	$4.0461187 \pm 1.32 \times 10^{-8}$	$(1.339 \pm 0.000) \times 10^{-3}$	-456.27992 ± 0.00097	3021.69 ± 0.21		
			5:1	$4.0460684 \pm 3.44 \times 10^{-8}$	$(1.316 \pm 0.000) \times 10^{-3}$	-460.0092 ± 0.0025	3073.7 ± 1.0		
		G395M	2:1	$4.0460094 \pm 1.89 \times 10^{-7}$	$(3.505 \pm 0.001) \times 10^{-3}$	-464.382 ± 0.014	1154.51 ± 0.18		
			3:1	$4.0460292 \pm 1.79 \times 10^{-7}$	$(3.225 \pm 0.001) \times 10^{-3}$	-462.910 ± 0.013	1254.50 ± 0.38		
			5:1	$4.0459141 \pm 4.20 \times 10^{-8}$	$(3.401 \pm 0.002) \times 10^{-3}$	-471.4390 ± 0.0031	1189.47 ± 0.67		
		PRISM	2:1	$4.0469642 \pm 6.28 \times 10^{-7}$	$(1.783 \pm 0.002) \times 10^{-2}$	-393.637 ± 0.046	226.93 ± 0.25		
			3:1	$4.0482463 \pm 2.96 \times 10^{-6}$	$(1.908 \pm 0.005) \times 10^{-2}$	-298.68 ± 0.22	212.17 ± 0.60		
			5:1	$4.0477221 \pm 2.14 \times 10^{-6}$	$(1.841 \pm 0.003) \times 10^{-2}$	-337.50 ± 0.16	219.81 ± 0.33		
			5:2	$4.0472306 \pm 6.47 \times 10^{-6}$	$(1.880 \pm 0.004) \times 10^{-2}$	-373.90 ± 0.48	215.28 ± 0.42		
			7:1	$4.0472962 \pm 3.86 \times 10^{-6}$	$(1.768 \pm 0.005) \times 10^{-2}$	-369.04 ± 0.29	228.96 ± 0.58		
			8:1	$4.0484607 \pm 4.76 \times 10^{-6}$	$(1.920 \pm 0.004) \times 10^{-2}$	-282.80 ± 0.35	210.81 ± 0.39		
Hu 7	4.1708031	G395H	2:1	$4.1644895 \pm 2.81 \times 10^{-7}$	$(1.889 \pm 0.001) \times 10^{-3}$	-454.160 ± 0.020	2205.0 ± 1.0		
			3:1	$4.1643313 \pm 1.49 \times 10^{-6}$	$(1.319 \pm 0.051) \times 10^{-3}$	-465.55 ± 0.11	3156 ± 123		
			5:1	$4.1642570 \pm 4.11 \times 10^{-7}$	$(1.625 \pm 0.014) \times 10^{-3}$	-470.902 ± 0.030	2563 ± 22		
		G395M	2:1	$4.1651728 \pm 1.91 \times 10^{-6}$	$(3.621 \pm 0.019) \times 10^{-3}$	-404.98 ± 0.14	1150.1 ± 6.1		
			3:1	$4.1645298 \pm 1.16 \times 10^{-5}$	$(3.875 \pm 0.066) \times 10^{-3}$	-451.26 ± 0.84	1075 ± 18		
HeI 42958	4.2957500	G395H	5:1	$4.1646173 \pm 6.17 \times 10^{-6}$	$(3.114 \pm 0.010) \times 10^{-3}$	-444.96 ± 0.44	1337.5 ± 4.4		
			2:1	$4.2894088 \pm 1.05 \times 10^{-7}$	$(1.307 \pm 0.004) \times 10^{-3}$	-442.8663 ± 0.0073	3281 ± 11		
			3:1	$4.2893880 \pm 8.13 \times 10^{-7}$	$(1.340 \pm 0.002) \times 10^{-3}$	-444.321 ± 0.057	3201.3 ± 5.7		
		G395M	5:1	$4.2893701 \pm 4.35 \times 10^{-7}$	$(1.334 \pm 0.005) \times 10^{-3}$	-445.570 ± 0.030	3215 ± 13		
			2:1	$4.2893609 \pm 6.30 \times 10^{-7}$	$(3.423 \pm 0.032) \times 10^{-3}$	-446.214 ± 0.044	1253 ± 12		
			3:1	$4.2894574 \pm 3.09 \times 10^{-6}$	$(3.046 \pm 0.031) \times 10^{-3}$	-439.47 ± 0.22	1408 ± 15		
		Hu 6	4.3764640	G395H	5:1	$4.2891298 \pm 3.98 \times 10^{-6}$	$(3.140 \pm 0.054) \times 10^{-3}$	-462.37 ± 0.28	1366 ± 24
					2:1	$4.3698988 \pm 8.09 \times 10^{-7}$	$(1.204 \pm 0.008) \times 10^{-3}$	-450.061 ± 0.055	3630 ± 25
					3:1	$4.3697745 \pm 1.16 \times 10^{-5}$	$(1.232 \pm 0.157) \times 10^{-3}$	-458.59 ± 0.79	3546 ± 451
				G395M	5:1	$4.3696240 \pm 6.06 \times 10^{-6}$	$(1.692 \pm 0.026) \times 10^{-3}$	-468.92 ± 0.42	2583 ± 39
					2:1	$4.3699338 \pm 8.50 \times 10^{-7}$	$(3.119 \pm 0.063) \times 10^{-3}$	-447.660 ± 0.058	1401 ± 28
					3:1	$4.3696465 \pm 1.86 \times 10^{-7}$	$(3.035 \pm 0.000) \times 10^{-3}$	-467.375 ± 0.013	1439.77 ± 0.18
[MgIV] 44867	4.4866800	G395M	5:1	$4.3691444 \pm 4.25 \times 10^{-6}$	$(3.541 \pm 0.037) \times 10^{-3}$	-501.82 ± 0.29	1234 ± 13		
			2:1	$4.4796650 \pm 1.43 \times 10^{-7}$	$(1.231 \pm 0.003) \times 10^{-3}$	-469.0965 ± 0.0095	3639.2 ± 9.6		
			3:1	$4.4796567 \pm 4.32 \times 10^{-8}$	$(1.271 \pm 0.001) \times 10^{-3}$	-469.6499 ± 0.0029	3525.1 ± 3.3		
			5:1	$4.4796461 \pm 1.67 \times 10^{-8}$	$(1.261 \pm 0.004) \times 10^{-3}$	-470.3610 ± 0.0011	3553 ± 12		
			2:1	$4.4796640 \pm 5.91 \times 10^{-7}$	$(3.217 \pm 0.004) \times 10^{-3}$	-469.163 ± 0.040	1392.5 ± 1.6		

Check with the JWST SOCCER Database at: <https://soccer.stsci.edu>

To verify that this is the current version.

Line	Lab λ (μm)	Grating	Obs.	Measured λ (μm)	Measured FWHM (μm)	Velocity Offset (km/s)	R
		PRISM	3:1	$4.4796975 \pm 6.72 \times 10^{-9}$	$(3.220 \pm 0.006) \times 10^{-3}$	-466.92056 ± 0.00045	1391.1 ± 2.7
			5:1	$4.4796215 \pm 1.54 \times 10^{-7}$	$(3.290 \pm 0.007) \times 10^{-3}$	-472.005 ± 0.010	1361.8 ± 2.8
			2:1	$4.4813060 \pm 3.92 \times 10^{-6}$	$(1.563 \pm 0.005) \times 10^{-2}$	-359.30 ± 0.26	286.75 ± 0.96
			3:1	$4.4822519 \pm 2.04 \times 10^{-6}$	$(1.566 \pm 0.007) \times 10^{-2}$	-296.02 ± 0.14	286.2 ± 1.4
			5:1	$4.4818941 \pm 2.36 \times 10^{-5}$	$(1.654 \pm 0.003) \times 10^{-2}$	-320.0 ± 1.6	270.90 ± 0.56
			5:2	$4.4813394 \pm 4.51 \times 10^{-7}$	$(1.590 \pm 0.003) \times 10^{-2}$	-357.064 ± 0.030	281.83 ± 0.50
			7:1	$4.4813758 \pm 3.35 \times 10^{-6}$	$(1.500 \pm 0.003) \times 10^{-2}$	-354.63 ± 0.22	298.76 ± 0.64
			8:1	$4.4822651 \pm 1.00 \times 10^{-6}$	$(1.622 \pm 0.002) \times 10^{-2}$	-295.144 ± 0.067	276.26 ± 0.35
Pf β	4.6537921	G395H	2:1	$4.6467641 \pm 2.10 \times 10^{-7}$	$(1.328 \pm 0.001) \times 10^{-3}$	-453.075 ± 0.014	3498.7 ± 2.4
			3:1	$4.6467328 \pm 6.28 \times 10^{-10}$	$(1.356 \pm 0.000) \times 10^{-3}$	-455.098467 ± 0.000040	3426.66 ± 0.99
			5:1	Wavelength Coverage Gap or No Fit			
		G395M	2:1	$4.6466787 \pm 3.52 \times 10^{-7}$	$(3.384 \pm 0.014) \times 10^{-3}$	-458.585 ± 0.023	1373.0 ± 5.6
			3:1	$4.6467123 \pm 4.90 \times 10^{-7}$	$(3.366 \pm 0.005) \times 10^{-3}$	-456.418 ± 0.032	1380.3 ± 1.9
			5:1	$4.6465736 \pm 2.53 \times 10^{-6}$	$(3.289 \pm 0.025) \times 10^{-3}$	-465.36 ± 0.16	1413 ± 11
		PRISM	2:1	$4.6478676 \pm 1.57 \times 10^{-6}$	$(1.544 \pm 0.016) \times 10^{-2}$	-381.89 ± 0.10	301.1 ± 3.1
			3:1	$4.6499720 \pm 1.25 \times 10^{-5}$	$(2.031 \pm 0.009) \times 10^{-2}$	-246.18 ± 0.80	229.0 ± 1.0
			5:1	$4.6496270 \pm 2.84 \times 10^{-4}$	$(1.908 \pm 0.022) \times 10^{-2}$	-268 ± 18	243.7 ± 2.8
			5:2	$4.6496725 \pm 7.46 \times 10^{-6}$	$(1.926 \pm 0.003) \times 10^{-2}$	-265.50 ± 0.48	241.44 ± 0.33
			7:1	$4.6495258 \pm 1.14 \times 10^{-6}$	$(1.952 \pm 0.012) \times 10^{-2}$	-274.955 ± 0.073	238.2 ± 1.4
			8:1	$4.6501202 \pm 5.34 \times 10^{-6}$	$(1.950 \pm 0.003) \times 10^{-2}$	-236.63 ± 0.34	238.43 ± 0.32
Hu ϵ	4.6725190	G395H	2:1	$4.6654046 \pm 5.22 \times 10^{-6}$	$(1.447 \pm 0.014) \times 10^{-3}$	-456.81 ± 0.34	3225 ± 31
			3:1	$4.6654157 \pm 3.16 \times 10^{-6}$	$(1.297 \pm 0.049) \times 10^{-3}$	-456.10 ± 0.20	3598 ± 135
			5:1	Wavelength Coverage Gap or No Fit			
HeII 47635	4.7635078	G395H	2:1	$4.7563534 \pm 3.58 \times 10^{-7}$	$(1.346 \pm 0.002) \times 10^{-3}$	-450.605 ± 0.023	3534.4 ± 4.9
			3:1	$4.7563193 \pm 7.55 \times 10^{-7}$	$(1.187 \pm 0.023) \times 10^{-3}$	-452.755 ± 0.048	4006 ± 76
			5:1	Wavelength Coverage Gap or No Fit			
		G395M	2:1	$4.7564486 \pm 6.06 \times 10^{-6}$	$(2.858 \pm 0.147) \times 10^{-3}$	-444.60 ± 0.38	1664 ± 85
			3:1	$4.7562697 \pm 3.11 \times 10^{-7}$	$(2.832 \pm 0.080) \times 10^{-3}$	-455.877 ± 0.020	1680 ± 47
			5:1	$4.7562873 \pm 2.12 \times 10^{-5}$	$(2.739 \pm 0.070) \times 10^{-3}$	-454.8 ± 1.3	1737 ± 44
Hu δ	5.1286688	G395H	2:1	$5.1208321 \pm 3.11 \times 10^{-6}$	$(1.321 \pm 0.024) \times 10^{-3}$	-458.44 ± 0.18	3877 ± 71
			3:1	$5.1208608 \pm 2.35 \times 10^{-6}$	$(1.392 \pm 0.011) \times 10^{-3}$	-456.76 ± 0.14	3678 ± 28
			5:1	Wavelength Coverage Gap or No Fit			
		G395M	2:1	$5.1209567 \pm 2.81 \times 10^{-5}$	$(4.044 \pm 0.044) \times 10^{-3}$	-451.1 ± 1.6	1266 ± 14
			3:1	$5.1207602 \pm 7.46 \times 10^{-6}$	$(4.153 \pm 0.058) \times 10^{-3}$	-462.65 ± 0.44	1233 ± 17
			5:1	$5.1208399 \pm 1.48 \times 10^{-5}$	$(4.801 \pm 0.107) \times 10^{-3}$	-457.98 ± 0.86	1067 ± 24
		PRISM	2:1	$5.1234553 \pm 3.59 \times 10^{-5}$	$(1.216 \pm 0.022) \times 10^{-2}$	-304.9 ± 2.1	421.4 ± 7.5
			3:1	$5.1231170 \pm 2.80 \times 10^{-5}$	$(1.498 \pm 0.003) \times 10^{-2}$	-324.7 ± 1.6	342.06 ± 0.61
			5:1	$5.1217568 \pm 5.58 \times 10^{-5}$	$(1.209 \pm 0.060) \times 10^{-2}$	-404.3 ± 3.3	424 ± 21
			5:2	$5.1227601 \pm 8.32 \times 10^{-5}$	$(1.463 \pm 0.006) \times 10^{-2}$	-345.6 ± 4.9	350.1 ± 1.3
			7:1	$5.1225176 \pm 6.50 \times 10^{-5}$	$(1.359 \pm 0.006) \times 10^{-2}$	-359.8 ± 3.8	377.0 ± 1.6
			8:1	$5.1229783 \pm 3.12 \times 10^{-6}$	$(1.692 \pm 0.011) \times 10^{-2}$	-332.82 ± 0.18	302.8 ± 2.0

Check with the JWST SOCCER Database at: <https://soccer.stsci.edu>
 To verify that this is the current version.

8 References

- Birkmann, S., Boker, T., Ferruit, P., Giardino, G., Jakobsen, P., de Marchi, G., Sirianni, M., te Plate, M., Savignol, J.C., Gnata, X., Wettemann, T., Dorner, B., Cresci, G., Rosales-Ortega, F., Stuhlinger, M., Cole, R., Tandy, J., & Brockley-Blatt, C. (2011). Wavelength calibration of the JWST near-infrared spectrograph (NIRSpec). In *Cryogenic Optical Systems and Instruments XIII* (pp. 81500B).
- Bushouse, H., Eisenhamer, J., Dencheva, N., Davies, J., Greenfield, P., Morrison, J., Hodge, P., Simon, B., Grumm, D., Droettboom, M., Slavich, E., Sosey, M., Pauly, T., Miller, T., Jedrzejewski, R., Hack, W., Davis, D., Crawford, S., Law, D., ... Filippazzo, J. (2025). JWST Calibration Pipeline (1.18.0). Zenodo. <https://doi.org/10.5281/zenodo.15178003>
- Galera-Rosillo, Rebeca, Mampaso, Antonio, Corradi, Romano L. M., García-Rojas, Jorge, Balick, Bruce, Jones, David, ... Villaver, Eva. (2022). On the most luminous planetary nebulae of M 31. *A&A*, 657, A71. doi:10.1051/0004-6361/202141890
- JWST User Documentation (JDox). Baltimore, MD: Space Telescope Science Institute; 2016-2023 April, 1. <https://jwst-docs.stsci.edu>
- Kniazev, A. Y., Grebel, E. K., Zucker, D. B., Rix, H.-W., Martínez-Delgado, D., & Snedden, S. A. (2014). A Search for Planetary Nebulae with the Sloan Digital Sky Survey: The Outer Regions of M31. *Aj*, 147(1), 16. <https://doi.org/10.1088/0004-6256/147/1/16>
- Kramida, A., Yu. Ralchenko, Reader, J., & and NIST ASD Team. (2024). NIST Atomic Spectra Database (ver. 5.12), [Online]. Available: <https://physics.nist.gov/asd> [2025, November 11]. National Institute of Standards and Technology, Gaithersburg, MD.
- Lützgendorf, N., Giardino, G., Oliveira, C., Zeidler, P., Ferruit, P., Jakobsen, P., Kumari, N., Rawle, T., Birkmann, S., Böker, T., Proffitt, C., Sirianni, M., Te Plate, M., & Sohn, S. (2022). Astrometric and wavelength calibration of the NIRSpec instrument during commissioning using a model-based approach. In *Space Telescopes and Instrumentation 2022: Optical, Infrared, and Millimeter Wave* (pp. 121800Y).